UNIVERSITY OF COPENHAGEN
FACULTY OF SCIENCE

3D Modelling of Turbulence in a Magnetically Confined Toroidal Plasma

Master Thesis

Aske Anguasak Busk Olsen

Niels Bohr Institute
Supervisor: Peter Ditlevsen, Jens Juul Rasmussen (DTU) and Jens Madsen (DTU)
Submitted: November 29, 2016

UNIVERSITY OF
COPENHAGEN

Faculty:	Science
Institute:	Niels Bohr Institute
Author:	Aske Anguasak Busk Olsen
Email:	*slz207@alumni.ku.dk*
Title and Subtitle:	3D Modelling of Turbulence in a Magnetically Confined Toroidal Plasma - Master Thesis
Supervisor:	Peter Ditlevsen, Jens Juul Rasmussen (DTU) and Jens Madsen (DTU)
Handed in:	November 29, 2016
Defended:	12/12-2016

Name ______________________

Signature ______________________

Date ______________________

Acknowledgements

I would like to thank my internal supervisor Peter Ditlevsen, and my external supervisors Jens Juul Rasmussen and Jens Madsen for guidance and always being helpful.

I want to dedicate a special thanks to the BOUT++ expert, of the PPFE group at DTU, Michael Løiten Magnussen for always being helpful and answering a lot of questions regarding the BOUT++ platform.

Finally I send a special thanks to my brother, Jeppe Miki Busk Olsen, for igniting my interest in plasma physics.

Abstract

Nuclear fusion has been proposed as an alternative clean energy source. In order to have a deep understanding of the dynamic properties of a fusion plasma an accurate model is needed. Most investigations of fusion plasmas have been done using two dimensional models, even though a realistic model involves dynamics in three dimensions.

This thesis sets out to create a coordinate system aligned with the magnetic field in order to create a realistic model in three dimensions whilst having a coarse resolution in the direction of the magnetic field.

Using the model created, an investigation of the Hasegawa-Wakatani equations was done. Three different cases were investigated using three different values of magnetic shear.

The simulations showed a dependence on the magnetic shear for the stability of the system which is in accordance theory. The field-aligned coordinate system created in this thesis shows promising results as the platform for future simulations in three dimensions.

Contents

Chapter 1

Introduction

1.1 Motivation

Since the beginning of the industrial revolution there has been an almost exponential growth in worldwide energy consumption, which has lead to an increase in emission of greenhouse gasses. Studies have shown a link between an increase of greenhouse gasses in the atmosphere and an increase in the global temperature. [1] The higher temperatures on earth can lead to more extreme weather conditions and more non-nutritious land. So unless something is done to stop the emission of greenhouse gasses the world stands before a potential environmental catastrophe.

Many steps have been, and are currently being taken, in order to reduce the emission of greenhouse gasses. Various forms of sustainable energy sources have been investigated. However most of the sustainable sources of energy have some problematic traits.

Wind energy works fine in countries such as Denmark, a country that is windy at almost all times. However even though wind energy might at times meet the needs of a country like Denmark, it is highly unreliable due to the chaotic nature of wind systems. At times where the windmills generate excessive power there is currently no efficient way of storing the energy, since most batteries are quite inefficient. Furthermore batteries consists of liquids that are harmful to the environment. Another issue with windmills is that they are only usable in windy countries. This means that windmills may be part of the solution for having 100% sustainable energy, but not the only solution.

A similar problem arises with hydroelectric plants, it is great in countries like Norway, a country with a lot of mountains that are necesarry in order for hydroelectric plants to work, however countries with no mountains can not rely on hydroelectric plants as the main energy source.

Solar cells rely on sunlight, and are, as windmills, unreliable. Furthermore current solar cells are fragile and easily broken.

In conclusion solar-, wind- and hydroelectric energy can not stand alone as environmentally sustainable energy sources, which means there is a need for other sustainable energy sources. Another source of energy that could potentially cover the global need is nuclear energy by fission. However a problem arises with storage of the radioactive waste, where the waste has a half-life of up to $\sim$ 200000 years [2]. Although discussion can be made as to whether or not the storage of the waste is an unsolvable problem there is still opposition among the general population towards nuclear fission.

This leads to one final solution to the energy crisis, which is nuclear fusion. There is radioactive waste from fusion reactions, however the amount of radioactive waste is not large, and the half-life of the waste is short ($\sim$12 years [3]) and the waste can be confined within the power plant, making transportation unnecessary. Working fusion reactors might be the solution to obtaining energy production based solely on sustainable energy due to the abundance on earth of the fuels used in a nuclear power plant.

1.2 Thermonuclear Fusion

A plasma is a gas consisting of ionized particles. The reaction of interest in a plasma used for fusion power is the one between tritium (^{3}H) and deuterium (^{2}H) [4]. Tritium can be obtained by splitting lithium, a common metal, and deuterium is found in water($\sim$ 0.0156% of the water [5]). The fusion between tritium and deuterium gives a high energy output [4], and as seen in figure 1.1, which is a plot of the cross sections of three different reactions as a function of temperature, it has the highest cross section between 10 and 100 keV deuteron energy of the three reactions shown (the cross section is a measure of the probability of the two fusing).

The reaction of interest is thus

$$^2_1\mathrm{H} + ^3_1\mathrm{H} \rightarrow ^4_2\mathrm{He} + \mathrm{n} \tag{1.1}$$

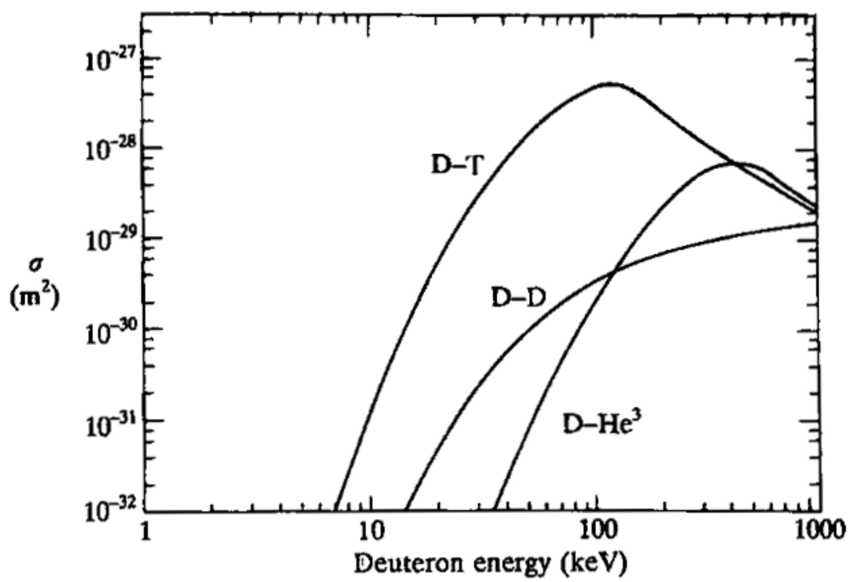

Figure 1.1: The cross section as a function of deuteron energy [4].

The system must conserve energy and momentum, allowing us to calculate the energy freed in the fusion process. The sum of the rest energy of tritium and deuterium can be subtracted from the sum of the rest energy of helium and a neutron. We know that the excessive energy must be stored in the momentum of the neutron and the momentum of the helium core. The rest energy is given by Einsteins equation [2]

$$\mathrm{E}_{rest} = mc^2 \tag{1.2}$$

The mass of deuterium is 2.01410178 u [2], the mass of tritium is 3.0160492 u, the mass of helium is 4.002602 u and the mass of the neutron is 1.008664 u. The energy freed is thus

$$2.01410178\mathrm{u} + 3.0160492\mathrm{u} - (4.002602\mathrm{u} + 1.008664\mathrm{u}) = 0.01888498\mathrm{u}$$

One atomic mass unit is equivalent to 931.494 $\frac{\mathrm{MeV}}{c}$ [2] and we have

$$0.01888498 \cdot 931.494\mathrm{MeV} = 17.6\mathrm{MeV}$$

freed energy per reaction. To achieve fusion, however, one must overcome the Coulomb barrier, which requires high temperatures [6]. As seen in figure 1.1 the ideal energy of the deuterons to maximize the number of collisions is ~ 100 keV. To convert electron volt to kelvin we multiply by $\frac{\mathrm{e}}{\mathrm{k}_B} \approx 11600$. The naive guess at the ideal temperature for fusion devices is thus $1.16 \cdot 10^9$K, however other factors must be taken in to account.

If the distribution of particles is Maxwellian, the reaction rate for deuterium-tritium reactions can be written as [4]

$$R = n_d n_t \langle \sigma v \rangle$$

where n_d and n_t is the amount of deuterium and tritium atoms respectively. The thermonuclear power per unit volume is then the reaction rate times the energy released per reaction [4]

$$p_T = n_d n_t \langle \sigma v \rangle \epsilon = (n - n_t) n_t \langle \sigma v \rangle \epsilon, \tag{1.3}$$

where the total ion density is $n = n_d + n_t$, since the helium cores contribute with almost nothing to the total density. It is seen that the thermonuclear power per unit volume is optimized when $n_d = n_t$ in which case the thermonuclear power per unit volume reads

$$p_T = \frac{1}{4} n^2 \langle \sigma v \rangle \epsilon$$

The total loss in the confined plasma is given by $W = 3\overline{nT}V$ [4], where the bar denotes an average, T is the plasma temperature and V is the volume. The rate of loss is expressed as [4]

$$P_L = \frac{W}{\tau_E}, \tag{1.4}$$

where τ_E is the energy confinement time. The alpha particle (helium core) is confined by the external magnetic field and the energy of the alpha particle stays in the system and is transferred to the other particles through collisions. After a collision fusing two particles about $\frac{4}{5}$ of the energy is in the neutron and the rest is in the alpha particle [4]. In order to have as much energy stay in the system as is lost, we must have

$$P_H + P_\alpha = P_L,$$

where P_H is an external power source, and P_α is the heating caused by the α-particles. The total α-particle heating can also be expressed as $\frac{1}{4}\overline{n^2\langle\sigma v\rangle}\epsilon_\alpha V$ [4], where the bar denotes an average, and ϵ_α is the energy carried by the α-particles.

It is possible to have all required heating of the plasma, come from the α-particle heating. When this is achieved it is called ignition. The ignition criteria is thus that $P_\alpha > P_L$ or

$$n\tau_E \geq \frac{12}{\langle\sigma v\rangle}\frac{T}{\epsilon_\alpha}, \tag{1.5}$$

where the bars have been omitted for convenience. The right hand side is only a function of temperature and a graph of $n\tau_E$ as a function of T can be seen in figure 1.2. As seen on the graph the minimum required $n\tau_E$ for ignition occurs at $T \sim 20$keV or at approximately 200 million degrees kelvin.

Since ignition is required for fusion devices as an energy source, the optimal temperature for a fusion device is at 20 keV. However no known solid material can withstand such temperatures, and another way of confining the plasma is needed. Luckily, a plasma consists of charged particles and can thus be confined by an external magnetic field. The two currently most promising devices, are the tokamak and the stellarator, where the focus in this thesis is on the tokamak.

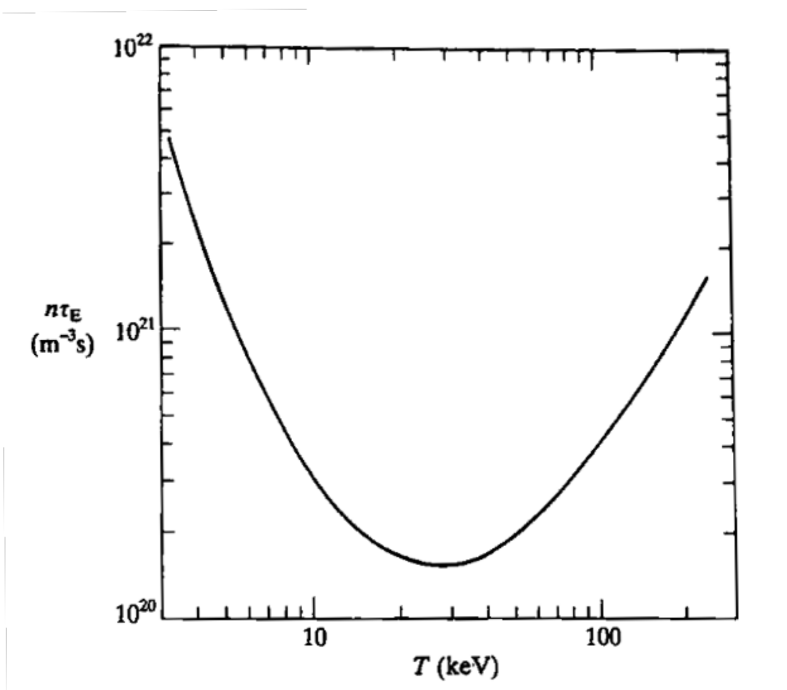

Figure 1.2: $n\tau_E$ as a function of T [4]

1.3 The Tokamak

The tokamak is a device for confining a plasma by the use of an external magnetic field. It is torus-shaped with magnetic coils surrounding it. In order to create a magnetic field that confines the plasma, both magnetic fields in the poloidal and toroidal directions are generated [4].

Figure 1.3 is a graphical illustration of a tokamak, showing the toroidal- and inner and outer poloidal coils, which result in twisted magnetic field lines in the plasma. The magnetic field of the tokamak is described in detail in chapter 4 and is a central part of understanding the dynamics of a magnetically confined plasma. The in depth handling of the subject is therefore left for the chapter. I will, however, give a brief introduction to the shape of the magnetic field.

The magnetic field can be expressed by a toroidal and poloidal part, with a toroidal field given by

$$\mathbf{B}_t = I(\psi)\nabla\phi,$$

where I is a function of the poloidal flux function, ψ, and ϕ is the toroidal angle, and the poloidal field given by

$$\mathbf{B}_p = \nabla\phi \times \nabla\psi. \tag{1.6}$$

Usually when touching the subject of a fusion plasma the analysis is centered around three different regions of the fusion plasma. The core region, where the magnetic field lines are closed, i.e. when the field lines will at some point close in on themselves, and form almost circular poloidal cross sections. The edge region that includes an X-point, which is the point at which the magnetic field lines go from closed to open. The X-point is sometimes called the separatrix. And finally a region of open field lines called the scrape of layer (SOL). Figure 1.4 shows the poloidal cross section of a tokamak, where the described regions can be seen. This thesis focuses on the edge region right before the X-point.

The shape of the magnetic field will be used to create a field-aligned coordinate system, used for simulating the Hasegawa-Wakatani equations, a simplified fluid model describing the dynamics a fusion plasma, and will create a platform with the possibility of simulating more complex equations in the future.

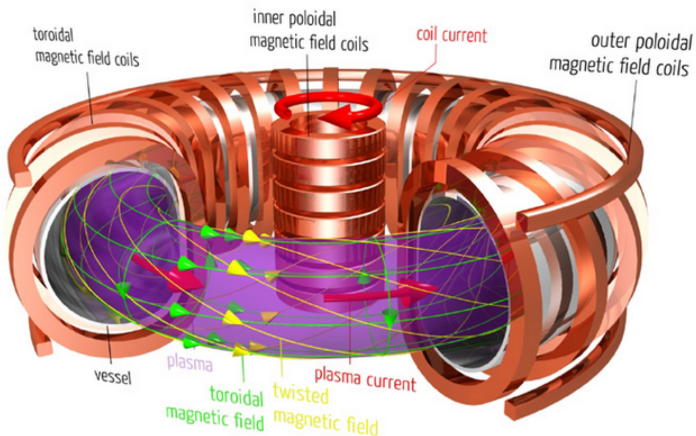

Figure 1.3: Graphical illustration of a tokamak [7].

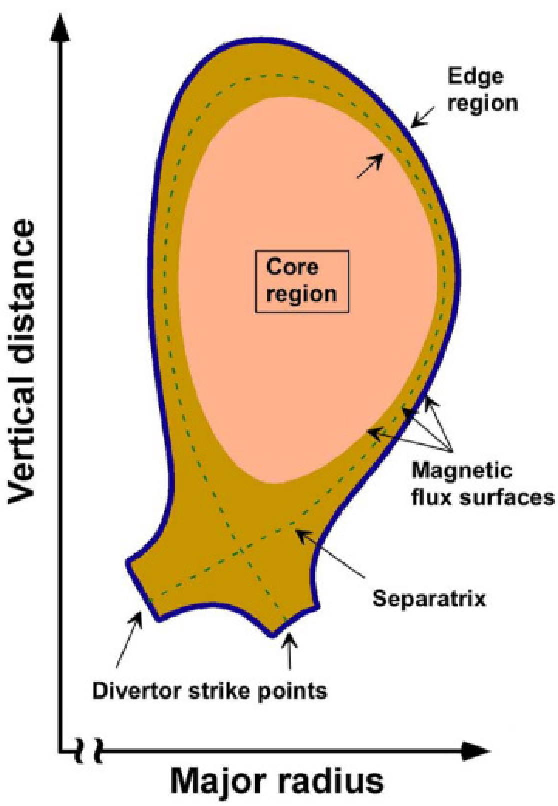

Figure 1.4: Poloidal cross section of a tokamak [8].

The outline of this thesis is as follows:

In chapter 2 a fluid description of fusion plasma dynamics is derived.

Chapter 3 gives a short description of the differential geometry used in this section

In chapter 4 a description of the shape of the magnetic field is described followed by a derivation of a set of coordinates aligned with the magnetic field.

In chapter 5 the Hasegawa-Wakatani model in curvilinear geometry is derived, by using simplifying assumptions on the fluid equations derived in chapter 2.

Chapter 6 describes the results of simulations perfomed for the Hasegawa-Wakatani model found in chapter 5.

And finally in chapter 7 we have the conclusion.

Chapter 2

The Two Fluid Equations

[1]A plasma usually consists of at least two species of particles and it is therefore convenient to describe a plasma in terms of these different species. In principle if the momenta and positions of all particles in a plasma are known at a given time, the behaviour of the plasma could be described exact. However a fusion plasma usually consists of more than 10^{24} particles of different species, making it impossible to simulate plasma properties using an individual particle model due to limited processing power, even if the initial momenta and positions of all particles are known.

It is therefore convenient to model a plasma differently, and it turns out that a plasma can be modelled as a fluid by using few assumptions.

2.1 The Vlasov Equation

In order to describe the evolution of a plasma we start by considering a point in one-dimensional phase space, which can be represented by the distribution function $f(x, v, t)$. Next, we examine a box in one-dimensional phase space of width dx and of height dv (see figure 2.1 [9]). Now the rate of change of particles in the one dimensional box can be described. The particle flux in the horizontal direction is given by $f(x, v, t)v$, where $v = \frac{dx}{dt}$ and in the vertical direction by $f(x, v, t)a$, where the acceleration $a = \frac{dv}{dt}$.

The flux into the left side of the box is given by the flux at x times the length of the side, so $f(x, v, t)vdv$, and into the right side at $x + dx$ with

[1]This chapter is a continuation of material written by me for a project in plasma physics.

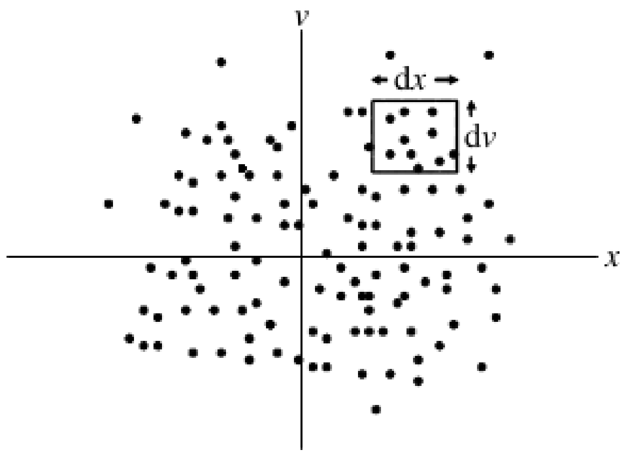

Figure 2.1: A box within phase-space having width dx and height dv. [9]

length dv it is given by $-f(x+dx,v,t)vdv$.

The flux into the bottom of the box at v with the length of the bottom being dx is $f(x,v,t)adx$, and into the top it is $-f(x,v+dv,t)adx$.

The total rate of change in the box will then be given by

$$\begin{aligned}\frac{\partial f(x,v,t)}{\partial t}dvdx = &-f(x+dx,v,t)vdv + f(x,v,t)vdv \\ &-f(x,v+dv,t)adx + f(x,v,t)adx \end{aligned} \tag{2.1}$$

Since we are in phase space v is independent of x, so all x operators commute with v and vice versa. Furthermore dividing by $dvdx$ and using

$$\lim_{dx\to 0}\frac{f(x+dx,v,t)v - f(x,v,t)v}{dx} = v\frac{\partial f(x,v,t)}{\partial x},$$

and

$$\lim_{dv\to 0}\frac{f(x,v+dv,t)a - f(x,v,t)a}{dv} = \frac{\partial(af(x,v,t))}{\partial v},$$

we arrive at the one dimensional Vlasov equation.

$$\frac{\partial f(x,v,t)}{\partial t} + v\frac{\partial f(x,v,t)}{\partial x} + \frac{\partial(af(x,v,t))}{\partial v} = 0. \tag{2.2}$$

This can be generalized to three dimensions [9]

$$\frac{\partial f(\mathbf{x},\mathbf{v},t)}{\partial t} + \mathbf{v}\frac{\partial f(\mathbf{x},\mathbf{v},t)}{\partial \mathbf{x}} + \frac{\partial(\mathbf{a} f(\mathbf{x},\mathbf{v},t))}{\partial \mathbf{v}} = 0.$$

The acceleration in the case of a plasma is given by the Lorentz force [9],

$$\mathbf{a} = \frac{q}{m}(\mathbf{E} + \mathbf{v} \times \mathbf{B}). \tag{2.3}$$

Since $(\mathbf{v} \times \mathbf{B})_i$ is perpendicular to v_i we have

$$\frac{\partial(\mathbf{v} \times \mathbf{B})_i}{\partial v_i} = 0,$$

meaning that $\frac{\partial}{\partial \mathbf{v}}$ and $\mathbf{a}$ commute. Using this, the Vlasov equation can be rewritten to

$$\frac{\partial f(\mathbf{x},\mathbf{v},t)}{\partial t} + \mathbf{v} \cdot \frac{\partial f(\mathbf{x},\mathbf{v},t)}{\partial \mathbf{x}} + \mathbf{a} \cdot \frac{\partial f(\mathbf{x},\mathbf{v},t)}{\partial \mathbf{v}} = 0. \tag{2.4}$$

2.1.1 Moments and collisions in the Vlasov equation

In the following section moments will be taken of the Vlasov equation to get a useful description of a two-fluid plasma. Taking moments is the procedure of multiplying f by powers of $\mathbf{v}$ and integrating it with respect to $\mathbf{v}$ [9]. Since we will be looking at the dynamics of different species, we denote f by its specie type σ as f_σ. To get the particle density in configuration space, we integrate the distribution function with respect to velocity in phase space,

$$n(\mathbf{x},t) = \int f_\sigma(\mathbf{x},\mathbf{v},t) d\mathbf{v}. \tag{2.5}$$

The mean velocity of the particles is given by

$$\mathbf{u} = \int \mathbf{v} \frac{f_\sigma(\mathbf{x},\mathbf{v},t)}{n(\mathbf{x},t)} d\mathbf{v}. \tag{2.6}$$

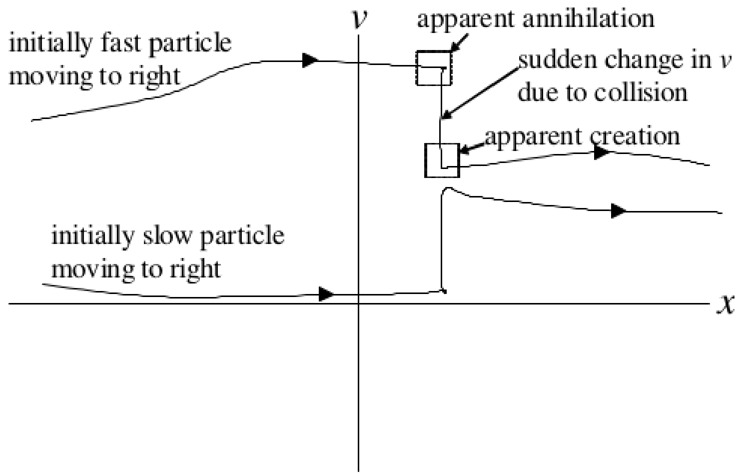

Figure 2.2: View of collisions in 1D phase space [9]

Collisions of two particles (nuclei and electrons) of different species changes the speed of the two particles significantly, whilst remaining at approximately the same position. An illustration of a collision can be seen in figure 2, and as seen from the figure you can view collisions as an annihilation of the colliding particles and the creation of two new [9]. The coupling of annihilation and creation rates constrains the form of the collision operator. Including collisions the Vlasov equation now takes the form:

$$\frac{\partial f_\sigma(\mathbf{x},\mathbf{v},t)}{\partial t} + \mathbf{v}\cdot\frac{\partial f_\sigma(\mathbf{x},\mathbf{v},t)}{\partial \mathbf{x}} + \mathbf{a}\cdot\frac{\partial f_\sigma(\mathbf{x},\mathbf{v},t)}{\partial \mathbf{v}} = \sum_\alpha C_{\sigma\alpha}(f_\sigma(\mathbf{x},\mathbf{v},t)) \quad (2.7)$$

Where $C_{\sigma\alpha}$ is the rate of change of f_σ due to collisions between particles of species σ with species α.

Constraints on the collision operator will help in the derivation of the moments of the Vlasov equation. The constraints on the collision operator are:

Constraint 1 Conservation of particles. A collision will not change the number of particles at a specific location (unless of course there is fusion, but even in high reaction plasmas, collisions where the two particles fuse are negligible on a large scale compared to other collisions).

$$\int d\mathbf{v} C_{\sigma\alpha}(f_\sigma) = 0 \tag{2.8}$$

Constraint 2 Conservation of momentum. As in all other physical situations momentum must be conserved.

$$\int d\mathbf{v} m_\sigma \mathbf{v} C_{\sigma\alpha}(f_\sigma) + \int d\mathbf{v} m_\alpha \mathbf{v} C_{\alpha\sigma}(f_\alpha) = 0 \tag{2.9}$$

Constraint 3 Conservation of energy. As in all other isolated physical systems energy must be conserved.

$$\int d\mathbf{v} m_\sigma v^2 C_{\sigma\alpha}(f_\sigma) + \int d\mathbf{v} m_\alpha v^2 C_{\alpha\sigma}(f_\alpha) = 0 \tag{2.10}$$

where $v^2 = \mathbf{v}\cdot\mathbf{v}$. With these constraints on the collision operator in mind, we are now able to take the first three moments of the Vlasov equation (0th, 1st and 2nd). Taking the zeroth moment we have

$$\int \left(\frac{\partial f_\sigma(\mathbf{x},\mathbf{v},t)}{\partial t} + \mathbf{v}\cdot \frac{\partial f_\sigma(\mathbf{x},\mathbf{v},t)}{\partial \mathbf{x}} + \mathbf{a}\cdot \frac{\partial f_\sigma(\mathbf{x},\mathbf{v},t)}{\partial \mathbf{v}} \right) d\mathbf{v} = \int d\mathbf{v} \sum_\alpha C_{\sigma\alpha}(f_\sigma(\mathbf{x},\mathbf{v},t)). \tag{2.11}$$

The derivatives of the first and second term of the left hand side both commute with the velocity integral, leaving us with an integral of the distribution function over all of velocity space. The right hand side gives zero due to our constraints on the collision operator. Evaluating the integral of the third term we have

$$\int_V d\mathbf{v} \nabla_v \cdot \mathbf{a} f_\sigma(\mathbf{x},\mathbf{v},t) = \int_S d\mathbf{s}\cdot \mathbf{a} f_\sigma(\mathbf{x},\mathbf{v},t) = 0. \tag{2.12}$$

In the above calculation gauss' law has been used, and the fact that $f(x,v,t)$ goes to zero as $\mathbf{v}$ goes to infinity makes the surface integral at infinity disappear. Furthermore using eq. (2.5) and (2.6) we have the zeroth moment:

$$\frac{\partial n_\sigma}{\partial t} + \nabla \cdot (n_\sigma \mathbf{u}_\sigma) = 0 \tag{2.13}$$

To get the first moment we multiply by the velocity on both sides of the Vlasov equation, eq. (2.7), and integrate with respect to $\mathbf{v}$.

$$\int \left(\mathbf{v}\frac{\partial f_\sigma(\mathbf{x},\mathbf{v},t)}{\partial t} + \mathbf{vv} \cdot \frac{\partial f_\sigma(\mathbf{x},\mathbf{v},t)}{\partial \mathbf{x}} + \mathbf{va} \cdot \frac{\partial f_\sigma(\mathbf{x},\mathbf{v},t)}{\partial \mathbf{v}} \right) d\mathbf{v}$$
$$= \int d\mathbf{v} \sum_\alpha C_{\sigma\alpha}(f_\sigma(\mathbf{x},\mathbf{v},t))\mathbf{v} \tag{2.14}$$

Now looking at each term individually, we have $\mathbf{u}_\sigma n_\sigma$ for the first term, as we found when deriving the equation for the 0th moment. For the second term we write the individual particle velocity $\mathbf{v}$ in terms of a flow velocity term, $\mathbf{u}_\sigma$, and a fluctuating velocity term, $\mathbf{v}'$, so $\mathbf{v} = \mathbf{v'} + \mathbf{u}_\sigma$, hence we also have $d\mathbf{v} = d\mathbf{v'}$. Rewriting the second term on the left hand side of eq. (2.14) we have

$$\frac{1}{\partial \mathbf{x}} \cdot \int \mathbf{vv} f_\sigma(\mathbf{x},\mathbf{v},t) d\mathbf{v} = \frac{1}{\partial \mathbf{x}} \cdot \int (\mathbf{v'v'} + \mathbf{u}_\sigma\mathbf{u}_\sigma + \mathbf{v'u}_\sigma + \mathbf{u}_\sigma\mathbf{v'}) f_\sigma(\mathbf{x},\mathbf{v},t) d\mathbf{v'} \tag{2.15}$$

Since the flow velocity is the total particle velocity, the integral over velocity space must be zero for any term including only one term of $\mathbf{v'}$ [9]. We define the pressure tensor as:

$$\overleftrightarrow{\mathbf{P}}_\sigma = m_\sigma \int \mathbf{v'v'} f_\sigma(\mathbf{x},\mathbf{v},t) d\mathbf{v'} \tag{2.16}$$

This gives for the second term on the left hand side of eq. (2.14):

$$\frac{1}{\partial \mathbf{x}} \cdot \left(\frac{1}{m_\sigma} \overleftrightarrow{\mathbf{P}}_\sigma + \mathbf{u}_\sigma\mathbf{u}_\sigma n_\sigma \right) \tag{2.17}$$

The last term on the left hand side of eq. (2.14) is

$$\int \mathbf{va} \cdot \frac{\partial f_\sigma(\mathbf{x},\mathbf{v},t)}{\partial \mathbf{v}} d\mathbf{v} \tag{2.18}$$

Using eq. (2.3) and integrating by parts whilst keeping in mind that the integral of the divergence of f is zero, we have

$$\begin{aligned}\int \mathbf{va} \cdot \frac{\partial f_\sigma(\mathbf{x},\mathbf{v},t)}{\partial \mathbf{v}} d\mathbf{v} &= \mathbf{v}\cdot 0 - \int \frac{\partial \mathbf{v}}{\partial \mathbf{v}} \cdot f_\sigma(\mathbf{x},\mathbf{v},t)\frac{q}{m}[\mathbf{E}+\mathbf{v}\times\mathbf{B}]d\mathbf{v} \\ &= -\int f_\sigma(\mathbf{x},\mathbf{v},t)\frac{q}{m}[\mathbf{E}+\mathbf{v}\times\mathbf{B}]d\mathbf{v}.\end{aligned} \tag{2.19}$$

Rewriting the velocity in terms of an average flow velocity and a random velocity, and using that the integral of terms involving the random velocity to the power of one is zero, we have

$$-\int f_\sigma(\mathbf{x},\mathbf{v},t)\frac{q_\sigma}{m_\sigma}[\mathbf{E}+\mathbf{u}_\sigma\times\mathbf{B}]d\mathbf{v} = -n_\sigma\frac{q_\sigma}{m_\sigma}[\mathbf{E}+\mathbf{u}_\sigma\times\mathbf{B}] \tag{2.20}$$

Finally we look at the collision term on the right hand side of eq. (2.14), where we introduce a frictional drag force, $\mathbf{R}_{\sigma\alpha}$ [9], which must be zero for $\sigma=\alpha$ since collisions between particles of the same species cannot change the total momentum of that species. The drag force is given by

$$\mathbf{R}_{\sigma\alpha} = \nu_{\sigma\alpha} m_\sigma n_\sigma(\mathbf{u}_\sigma - \mathbf{u}_\alpha) \tag{2.21}$$

which leaves us with an equation for the first moment of the Vlasov equation

$$\mathbf{u}_\sigma n_\sigma + \frac{1}{\partial \mathbf{x}} \cdot \left(\frac{1}{m_\sigma}\overset{\leftrightarrow}{\mathbf{P}}_\sigma + \mathbf{u}_\sigma\mathbf{u}_\sigma n_\sigma\right) - n_\sigma\frac{q_\sigma}{m_\sigma}[\mathbf{E}+\mathbf{u}_\sigma\times\mathbf{B}] = -\frac{1}{m_\sigma}\mathbf{R}_{\sigma\alpha} \tag{2.22}$$

which is usually multiplied by m_σ and rewritten as [9]

$$m_\sigma\left[\frac{\partial(n_\sigma\mathbf{u}_\sigma)}{\partial t} + \frac{\partial}{\partial \mathbf{x}}\cdot(n_\sigma\mathbf{u}_\sigma\mathbf{u}_\sigma)\right] = n_\sigma q_\sigma(\mathbf{E}+\mathbf{u}_\sigma\times\mathbf{B}) - \frac{\partial}{\partial \mathbf{x}}\cdot\overset{\leftrightarrow}{\mathbf{P}}_\sigma - \mathbf{R}_{\sigma\alpha}. \tag{2.23}$$

To calculate the second moment of the Vlasov equation we first make a simplifying assumption of the pressure tensor. The assumption is that $f_\sigma(\mathbf{x}, \mathbf{v}, t)$ is isotropic, in which case only the diagonal terms of the pressure tensor are non-zero. For that case we define the scalar pressure

$$\begin{aligned} P_\sigma &= m_\sigma \int v'_x v'_x f_\sigma(\mathbf{x}, \mathbf{v}, t) d\mathbf{v}'_\sigma = m_\sigma \int v'_y v'_y f_\sigma(\mathbf{x}, \mathbf{v}, t) d\mathbf{v}'_\sigma \\ &= m_\sigma \int v'_z v'_z f_\sigma(\mathbf{x}, \mathbf{v}, t) d\mathbf{v}'_\sigma = \frac{m_\sigma}{3} \int \mathbf{v}'_\sigma \cdot \mathbf{v}'_\sigma f_\sigma(\mathbf{x}, \mathbf{v}, t) d\mathbf{v}'. \end{aligned} \tag{2.24}$$

Sometimes it is convenient to work with systems of reduced dimensionality, where the scalar pressure can be generalized to [9]

$$P_\sigma = \frac{m_\sigma}{N} \int \mathbf{v}'_\sigma \cdot \mathbf{v}'_\sigma f_\sigma(\mathbf{x}, \mathbf{v}, t) d^N v' \tag{2.25}$$

where N is the number of dimensions.

We now take the second moment of the Vlasov equation, by multiplying with $m_\sigma \frac{v^2}{2}$ and integrating with respect to the velocity on both sides. This time, however, we integrate with respect to an N-dimensional velocity space.

$$\begin{aligned} \int \left(\frac{\partial}{\partial t} \frac{m_\sigma v^2}{2} f_\sigma(\mathbf{x}, \mathbf{v}, t) + \frac{\partial}{\partial \mathbf{x}} \cdot \frac{m_\sigma v^2}{2} \mathbf{v} f_\sigma(\mathbf{x}, \mathbf{v}, t) \right. \\ \left. + q_\sigma \frac{v^2}{2} \frac{\partial}{\partial \mathbf{v}} \cdot (\mathbf{E} + \mathbf{v} \times \mathbf{B}) f_\sigma(\mathbf{x}, \mathbf{v}, t) \right) d^N \mathbf{v} \\ = \sum_\sigma \int \frac{m_\sigma v^2}{2} f_\sigma(\mathbf{x}, \mathbf{v}, t) C_{\sigma\alpha} d^N \mathbf{v} \end{aligned} \tag{2.26}$$

To derive something useful, it is convenient to once again look at the individual parts of the equation. Using $\mathbf{v} = \mathbf{u}_\sigma + \mathbf{v}'$ throughout we have the first term

$$\int \frac{\partial}{\partial t} \frac{m_\sigma (\mathbf{u}_\sigma + \mathbf{v}')^2}{2} f_\sigma(\mathbf{x}, \mathbf{v}, t) d^N \mathbf{v} = \frac{\partial}{\partial t} \left(\frac{n_\sigma m_\sigma u_\sigma^2}{2} + \frac{N P_\sigma}{2} \right) \tag{2.27}$$

Using eq. (2.24) and (2.25) and introducing the heat flux $\mathbf{Q}_\sigma = \int \frac{m_\sigma v'^2}{2} \mathbf{v}' f_\sigma d^N \mathbf{v}$ we get for the second term on the left hand side of eq. (2.26)

$$\frac{\partial}{\partial \mathbf{x}} \cdot \int \frac{m_\sigma(\mathbf{u}_\sigma + \mathbf{v}')^2}{2}(\mathbf{u}_\sigma + \mathbf{v}') f_\sigma(\mathbf{x}, \mathbf{v}, t) d^N\mathbf{v} = \nabla \cdot \left(\mathbf{Q}_\sigma + \frac{2+N}{2} P_\sigma \mathbf{u}_\sigma + \frac{m_\sigma n_\sigma u_\sigma^2}{2} \mathbf{u}_\sigma \right) \tag{2.28}$$

Integrating by parts and recalling that the integral of the divergence of f is zero, and that $\mathbf{v} \times \mathbf{B}$ must be perpendicular to $\mathbf{v}$ we get for the third term on the left hand side of eq. (2.28)

$$\int \left(q_\sigma \frac{v^2}{2} \frac{\partial}{\partial \mathbf{v}} \cdot (\mathbf{E} + \mathbf{v} \times \mathbf{B}) f_\sigma(\mathbf{x}, \mathbf{v}, t) \right) d^N\mathbf{v} = -q_\sigma \int \mathbf{v} \cdot \mathbf{E} f_\sigma(\mathbf{x}, \mathbf{v}, t) d^N\mathbf{v} \tag{2.29}$$

$$= -q_\sigma \int (\mathbf{u}_\sigma + \mathbf{v}') \cdot \mathbf{E} f_\sigma(\mathbf{x}, \mathbf{v}, t) d^N\mathbf{v}' = -q_\sigma n_\sigma \mathbf{u}_\sigma \cdot \mathbf{E} \tag{2.30}$$

Finally we look at the collision term on the right hand side. From (2.9) we know that only terms where $\sigma \neq \alpha$ gives a non-zero value, and what is left corresponds to the energy transfer from species σ to species α denoted by $-(\frac{\partial W}{\partial t})_{E\sigma\alpha}$. The second moment is thus given by

$$\frac{\partial}{\partial t} \left(\frac{n_\sigma m_\sigma u_\sigma^2}{2} + \frac{N P_\sigma}{2} \right) + \nabla \cdot \left(\mathbf{Q}_\sigma + \frac{2+N}{2} P_\sigma \mathbf{u}_\sigma + \frac{m_\sigma n_\sigma u_\sigma u_\sigma^2}{2} \mathbf{u}_\sigma \right) \tag{2.31}$$
$$-q_\sigma n_\sigma \mathbf{u}_\sigma \cdot \mathbf{E} = -\left(\frac{\partial W}{\partial t} \right)_{E\sigma\alpha}$$

By introducing the convective derivative,

$$\frac{d}{dt} = \frac{\partial}{\partial t} + \mathbf{u}_\sigma \cdot \frac{\partial}{\partial \mathbf{x}}, \tag{2.32}$$

we can rewrite both the first and second moment of the Vlasov equation.

Using the relation found from eq. (2.13) and expanding the derivatives on the left hand side we can rewrite the first moment eq. (2.23) (where the pressure tensor has been replaced by the scalar pressure) to

$$n_\sigma m_\sigma \frac{d\mathbf{u}_\sigma}{dt} = n_\sigma q_\sigma \left(\mathbf{E} + \mathbf{u}_\sigma \times \mathbf{B}\right) - \nabla P_\sigma - \mathbf{R}_{\sigma\alpha} \tag{2.33}$$

In the second moment the terms with the velocity squared can be collected on the left hand side and rewritten by using the convective derivative. To simplify the second moment further, both sides of the first moment of the Vlasov equation is dotted with $\mathbf{u}_\sigma$.

$$\mathbf{u}_\sigma \cdot n_\sigma m_\sigma \frac{d\mathbf{u}_\sigma}{dt} = \mathbf{u}_\sigma \cdot \left(n_\sigma q_\sigma (\mathbf{E} + \mathbf{u}_\sigma \times \mathbf{B}) - \nabla P_\sigma - \mathbf{R}_{\sigma\alpha}\right) \tag{2.34}$$

Using the vector relation

$$\nabla(\mathbf{u}_\sigma \cdot \mathbf{u}_\sigma) = 2\mathbf{u}_\sigma \times (\nabla \times \mathbf{u}_\sigma) + 2(\mathbf{u}_\sigma \cdot \nabla)\mathbf{u}_\sigma \tag{2.35}$$

we have

$$\begin{aligned} n_\sigma m_\sigma \left[\frac{\partial}{\partial t}\left(\frac{u_\sigma^2}{2}\right) + \mathbf{u}_\sigma \cdot \left(\nabla\left(\frac{u_\sigma^2}{2}\right) - \mathbf{u}_\sigma \times \nabla \times \mathbf{u}_\sigma\right)\right] \\ = n_\sigma q_\sigma \mathbf{u}_\sigma \cdot \mathbf{E} - \mathbf{u}_\sigma \cdot \nabla P - \mathbf{R}_{\sigma\alpha} \cdot \mathbf{u}_\sigma \end{aligned} \tag{2.36}$$

this leaves us with an expression for the second moment of the Vlasov equation which reads

$$\frac{N}{2}\frac{dP_\sigma}{dt} + \frac{2+N}{2} P \nabla \cdot \mathbf{u}_\sigma = -\nabla \cdot \mathbf{Q}_\sigma + \mathbf{R}_{\sigma\alpha} \cdot \mathbf{u}_\sigma - \left(\frac{\partial W}{\partial t}\right)_{E\sigma\alpha} \tag{2.37}$$

The derived equations are what is typically called the two-fluid equations [9].

In summary we have three two-fluid equations. The equation describing the zeroth moment (2.13) is also called the continuity equation, the equation describing the first moment (2.33) is called the momentum conservation equation or often referred to as the equation of motion, and finally the equation describing the second moment (2.37) is also called the energy conservation equation or often referred to as the energy evolution equation.

So in summary we have the continuity equation

$$\frac{\partial n_\sigma}{\partial t} + \nabla \cdot (n_\sigma \mathbf{u}_\sigma) = 0, \tag{2.38}$$

the momentum conservation equation

$$n_\sigma m_\sigma \frac{d\mathbf{u}_\sigma}{dt} = n_\sigma q_\sigma (\mathbf{E} + \mathbf{u}_\sigma \times \mathbf{B}) - \nabla P_\sigma - R_{\sigma\alpha} \tag{2.39}$$

and the energy conservation equation

$$\frac{N}{2}\frac{dP_\sigma}{dt} + \frac{2+N}{2} P \nabla \cdot \mathbf{u}_\sigma = -\nabla \cdot \mathbf{Q}_\sigma + \mathbf{R}_{\sigma\alpha} \cdot \mathbf{u}_\sigma - (\frac{\partial W}{\partial t})_{E\sigma\alpha} \tag{2.40}$$

2.2 The closure problem

In the previous section three equations were derived describing the averaged evolution of two species of charged particles, however the continuity equation requires us to find a solution for $\mathbf{u}_\sigma$, which can be found using the momentum conservation equation, which in turn requires a solution for the pressure tensor to be found, which exists in the energy conservation equation, which requires a solution for the heat flux, which can be found taking the third moment of the Vlasov equation. However taking the third moment will give another term appearing in the fourth moment, and this will continue indefinitely and is called the closure problem. To close the set of equations we can take the adiabatic, or the isothermal limit of the second moment [9]. In the isothermal limit the heat flux term dominates all the other terms, and the temperature becomes isotropic. In the adiabatic limit the left hand side terms dominates the right hand side terms of eq. (2.40).

For the adiabatic limit we have

$$\frac{N}{2}\frac{dP_\sigma}{dt} = -\frac{2+N}{2} P_\sigma \cdot \nabla \mathbf{u}_\sigma \tag{2.41}$$

Using the continuity equation and defining $\gamma = \frac{N+2}{N}$ we get

$$\frac{1}{P_\sigma}\frac{dP_\sigma}{dt} = \frac{\gamma}{n_\sigma}\frac{dn_\sigma}{dt} \Leftrightarrow \tag{2.42}$$
$$\ln(P_\sigma) = g\ln(n_\sigma)\gamma \Leftrightarrow \tag{2.43}$$
$$P_\sigma = kn_\sigma^\gamma \tag{2.44}$$

where g is an integration constant. For the isothermal limit we simply use the ideal gas law to find the pressure, hence

$$P_\sigma = \kappa n_\sigma T_\sigma \tag{2.45}$$

Now we have a closed set of equations, however we do not yet have an expression for the fluid velocity.

2.3 Drift Equations

In this subsection we derive the drift (velocity) equations for a charged fluid in a slowly varying electromagnetic field.

The drift velocities are obtained by solving the momentum equation iteratively and the simplest solution is found by assuming that the electric and magnetic fields are constant in time. It is a good assumption that the momentum equations can be solved iteratively if the magnetic and electric fields are slowly varying. [6] Assuming that the timescale of the collisions is on the same order of the slowly varying fields in terms of the small parameter δ, the momentum equation, eq. (2.39), reads

$$0 = \mathbf{E} + \mathbf{u}_{\sigma 0} \times \mathbf{B} - \frac{\nabla P_\sigma}{n_\sigma q_\sigma}. \tag{2.46}$$

Crossing all terms with $\mathbf{B}$ on the right grants a solution reading

$$\mathbf{u}_{\sigma 0} = \frac{\mathbf{E}\times\mathbf{B}}{B^2} - \frac{\nabla P_\sigma \times \mathbf{B}}{n_\sigma q_\sigma B^2} \tag{2.47}$$

We now have the 0th order solution, where the first term on the right hand side is called the $\mathbf{E}\times\mathbf{B}$-drift and the second term is called the diamagnetic drift. The solution can then be plugged in to the left side of the momentum equation and solved using the same procedure giving a correction of order δ. This procedure can be done iteratively to n'th order. However, in this thesis we only do it to 1st order. We find the first order drift to be

$$\mathbf{u}_{\sigma 1} = -\frac{m_i}{eB^2}(\partial_t(\mathbf{u}_{\sigma 0} \times \mathbf{B}) + (\mathbf{u}_{\sigma 0} \cdot \nabla)(\mathbf{u}_{\sigma 0} \times \mathbf{B})) + \frac{\mathbf{E} \times \mathbf{B}}{B^2} - \frac{\nabla P_\sigma \times \mathbf{B}}{n_\sigma q_\sigma B^2} \tag{2.48}$$

Together with the two fluid equations (eqns. (2.38)-(2.40)) and either the adiabatic (eq. (2.44)) or the isothermal (eq. (2.45)) limit we have a way of describing a fusion plasma with a closed set of differential equations.

Chapter 3

Differential Geometry

In order to accurately simulate the 3-dimensional behaviour of a fusion plasma it is convenient to describe the equations governing the behaviour in a curvilinear geometry. This chapter will give a brief explanation of the differential geometry used to derive the curvilinear field-aligned coordinates.

3.1 Contra- and Covariant vectors

A term often used in differential geometry is contra- and covariant tensors. To explain the concept of these, we start by defining a set of reciprogal vectors.

Imagine we have a set of vectors $\mathbf{A}$, $\mathbf{B}$ and $\mathbf{C}$, and another set of vectors $\mathbf{a}$, $\mathbf{b}$ and $\mathbf{c}$. If

$$\mathbf{A} \cdot \mathbf{a} = \mathbf{B} \cdot \mathbf{b} = \mathbf{C} \cdot \mathbf{c} = 1, \tag{3.1}$$

and

$$\mathbf{A} \cdot \mathbf{b} = \mathbf{A} \cdot \mathbf{c} = \mathbf{B} \cdot \mathbf{a} = \mathbf{B} \cdot \mathbf{c} = \mathbf{C} \cdot \mathbf{a} = \mathbf{C} \cdot \mathbf{b} = 0 \tag{3.2}$$

the two sets are said to be reciprogal [10].

Since $\mathbf{a} \cdot \mathbf{B} = \mathbf{a} \cdot \mathbf{C} = 0$, $\mathbf{a}$ must be orthogonal to $\mathbf{B}$ and $\mathbf{C}$. We then know that $\mathbf{a}$ can be written as $\mathbf{a} = K\mathbf{B} \times \mathbf{C}$ where K is some constant. We also know that $\mathbf{a} \cdot \mathbf{A} = 1$, which means that the constant is found to be

$K = (\mathbf{A}\cdot(\mathbf{B}\times\mathbf{C}))^{-1}$. The same procedure can be followed to find expressions for **b** and **c**. Writing out the derived expressions for **a**, **b** and **c** in terms of **A**, **B** and **C** we have:

$$\mathbf{a} = \frac{\mathbf{B}\times\mathbf{C}}{\mathbf{A}\cdot(\mathbf{B}\times\mathbf{C})} \tag{3.3}$$

$$\mathbf{b} = \frac{\mathbf{C}\times\mathbf{A}}{\mathbf{B}\cdot(\mathbf{C}\times\mathbf{A})} \tag{3.4}$$

$$\mathbf{c} = \frac{\mathbf{A}\times\mathbf{B}}{\mathbf{C}\cdot(\mathbf{A}\times\mathbf{B})} \tag{3.5}$$

A similar expression can be written for **A**, **B** and **C** in terms of **a**, **b** and **c**, by interchanging **a** with **A**, **b** with **B** and **c** with **C**. Any vector can be written as a linear combination of a reciprogal set [10].

Now consider a transformation $\mathbf{R}(u^1, u^2, u^3)$, where a point determined by the position vector **R** is given by a function of three curvilinear coordinates u^1, u^2 and u^3. **R** can now be expanded in terms of its cartesian components

$$\mathbf{R}: \begin{array}{l} x(u^1, u^2, u^3) \\ y(u^1, u^2, u^3) \\ z(u^1, u^2, u^3) \end{array} \tag{3.6}$$

If the transformation is one-to-one it can be inverted and thus

$$\begin{array}{l} u^1(x, y, z) \\ u^2(x, y, z) \\ u^3(x, y, z) \end{array} \tag{3.7}$$

Hence the point **R** can be described uniquely by u^1, u^2 and u^3. We now set out to define a reciprogal basis set at the point u^1, u^2, u^3 determined by the position vector, **R**.

We start by defining a tangent basis e_1 along a coordinate curve (a coordinate curve is found by holding two coordinates fixed, whilst letting only one vary). We choose the tangent basis vectors to be $\frac{\partial\mathbf{R}}{\partial u^i}$ [10], hence:

$$e_1 = \frac{\partial\mathbf{R}}{\partial u^1}, e_2 = \frac{\partial\mathbf{R}}{\partial u^2}, e_3 = \frac{\partial\mathbf{R}}{\partial u^3} \tag{3.8}$$

Note that this coordinate basis is local, and in general the derivative of $\mathbf{R}$ with respect to u^i varies from one point in space to another point in space [10]. We now find the reciprogal basis vectors in order to be able to express any local vector as a linear combination of our set of basis vectors. The gradient of a function ϕ is defined such that the differential of the function $d\phi$ is given by $d\phi = \nabla\phi \cdot d\mathbf{R}$, which means that

$$du^i = \nabla u^i \cdot \mathbf{R} \tag{3.9}$$

using the chain rule $d\mathbf{R} = \frac{\partial \mathbf{R}}{\partial u^j} du^j = e_j du^j$ we have

$$du^i = \nabla u^i \cdot e_j du^j \tag{3.10}$$

which means that

$$\nabla u^i \cdot e_j = \delta^i_j \tag{3.11}$$

and hence a set of reciprogal basis vectors given by

$$e^i = \nabla u^i \tag{3.12}$$

From eq. (3.3)-(3.5) we must also have

$$e^1 = \nabla u^1 = \frac{e_2 \times e_3}{e_1 \cdot (e_2 \times e_3)} = \frac{\frac{\partial \mathbf{R}}{\partial u^2} \times \frac{\partial \mathbf{R}}{\partial u^3}}{\frac{\partial \mathbf{R}}{\partial u^1} \cdot (\frac{\partial \mathbf{R}}{\partial u^2} \times \frac{\partial \mathbf{R}}{\partial u^3})} \tag{3.13}$$

$$e^2 = \nabla u^2 = \frac{e_3 \times e_1}{e_2 \cdot (e_3 \times e_1)} = \frac{\frac{\partial \mathbf{R}}{\partial u^3} \times \frac{\partial \mathbf{R}}{\partial u^1}}{\frac{\partial \mathbf{R}}{\partial u^2} \cdot (\frac{\partial \mathbf{R}}{\partial u^3} \times \frac{\partial \mathbf{R}}{\partial u^1})} \tag{3.14}$$

$$e^3 = \nabla u^3 = \frac{e_1 \times e_2}{e_3 \cdot (e_1 \times e_2)} = \frac{\frac{\partial \mathbf{R}}{\partial u^1} \times \frac{\partial \mathbf{R}}{\partial u^2}}{\frac{\partial \mathbf{R}}{\partial u^3} \cdot (\frac{\partial \mathbf{R}}{\partial u^1} \times \frac{\partial \mathbf{R}}{\partial u^2})} \tag{3.15}$$

In general basis vectors with indecies down are called tangent basis vectors, and basis vectors with indecies up are called reciprogal basis vectors [10].

As stated earlier all vectors can be written as a linear combination of the reciprogal vector set. Hence a vector, $\mathbf{D}$, can be written as

$$\mathbf{D} = (\mathbf{D} \cdot \mathbf{a})\mathbf{A} + (\mathbf{D} \cdot \mathbf{b})\mathbf{B} + (\mathbf{D} \cdot \mathbf{c})\mathbf{C} \tag{3.16}$$

or

$$\mathbf{D} = (\mathbf{D} \cdot \mathbf{A})\mathbf{a} + (\mathbf{D} \cdot \mathbf{B})\mathbf{b} + (\mathbf{D} \cdot \mathbf{C})\mathbf{c} \tag{3.17}$$

In the case with our set of reciprogal basis vectors we can write

$$\mathbf{D} = (\mathbf{D} \cdot \mathbf{e}_1)\mathbf{e}^1 + (\mathbf{D} \cdot \mathbf{e}_2)\mathbf{e}^2 + (\mathbf{D} \cdot \mathbf{e}_3)\mathbf{e}^3 \tag{3.18}$$

and

$$\mathbf{D} = (\mathbf{D} \cdot \mathbf{e}^1)\mathbf{e}_1 + (\mathbf{D} \cdot \mathbf{e}^2)\mathbf{e}_2 + (\mathbf{D} \cdot \mathbf{e}^3)\mathbf{e}_3 \tag{3.19}$$

rewriting the scalars in the parenthesis as $(\mathbf{D} \cdot \mathbf{e}^i) = D^i$ and $(\mathbf{D} \cdot \mathbf{e}_i) = D_i$ we have

$$\mathbf{D} = D^i \mathbf{e}_i \tag{3.20}$$

$$\mathbf{D} = D_i \mathbf{e}^i \tag{3.21}$$

where repeated indices imply the einstein summing convention. The coefficients with the indices as subscripts, D_i, are called the covariant coefficients of the vector and the coefficients with the indices as superscripts, D^i , are called the contravariant coefficients of the vector [10]. In the rest of this thesis they are simply reffered to as the covariant and contravariant vectors for convenience.

3.2 The Metric and the Jacobian

In this section the metric and the jacobian will be defined. At the end of this section all vector operators used in this thesis will be stated for curvilinear geometry. For a more thorough explanation and derivations of the vector operators in curvilinear geometry see [10], [11] or other textbooks on the subject.

In order to write curvilinear operators on a simple form it is convenient to define a metric, which is a second order tensor including all necessary information about the curvature of the system [10]. The metric can be either covariant with indecies down, or contravariant with indecies up. The coefficients of the covariant metric is defined as [10]

$$g_{ij} = \mathbf{e}_i \cdot \mathbf{e}_j = \frac{\partial \mathbf{R}}{\partial u^i} \cdot \frac{\partial \mathbf{R}}{\partial u^j} \tag{3.22}$$

and for the contravariant [10]

$$g^{ij} = \mathbf{e}^i \cdot \mathbf{e}^j = \nabla u^i \cdot \nabla u^j \tag{3.23}$$

according to eqns. (3.13)-(3.15) the covariant metric components can be expressed in terms of the contravariant basis vectors and vice versa.

The Jacobian of the system is defined as the nine partial derivatives of a set of coordinates (x, y, z) with respect to another set of coordinates (u^1, u^2, u^3) [10]. So

$$\mathbf{J} = \begin{bmatrix} \frac{\partial x}{\partial u^1} & \frac{\partial y}{\partial u^1} & \frac{\partial z}{\partial u^1} \\ \frac{\partial x}{\partial u^2} & \frac{\partial y}{\partial u^2} & \frac{\partial z}{\partial u^2} \\ \frac{\partial x}{\partial u^3} & \frac{\partial y}{\partial u^3} & \frac{\partial z}{\partial u^3} \end{bmatrix} \tag{3.24}$$

In this thesis we are more often interested in the determinant of the Jacobian and for convience we will refer to the determinant of the Jacobian as the Jacobian from now on.

The Jacobian can be expressed in terms of the determinant of the metric. The covariant metric components can be seen as the matrix product of the two matrices $\frac{\partial \mathbf{R}}{\partial u^i}$ and $\frac{\partial \mathbf{R}}{\partial u^j}$, using that the determinant of a matrix product is the same as the product of the determinants we have

$$\det(g) = \det\left(\frac{\partial \mathbf{R}}{\partial u^i}\right) \det\left(\frac{\partial \mathbf{R}}{\partial u^j}\right) = \det \begin{bmatrix} \frac{\partial x}{\partial u^1} & \frac{\partial y}{\partial u^1} & \frac{\partial z}{\partial u^1} \\ \frac{\partial x}{\partial u^2} & \frac{\partial y}{\partial u^2} & \frac{\partial z}{\partial u^2} \\ \frac{\partial x}{\partial u^3} & \frac{\partial y}{\partial u^3} & \frac{\partial z}{\partial u^3} \end{bmatrix} \det \begin{bmatrix} \frac{\partial x}{\partial u^1} & \frac{\partial y}{\partial u^1} & \frac{\partial z}{\partial u^1} \\ \frac{\partial x}{\partial u^2} & \frac{\partial y}{\partial u^2} & \frac{\partial z}{\partial u^2} \\ \frac{\partial x}{\partial u^3} & \frac{\partial y}{\partial u^3} & \frac{\partial z}{\partial u^3} \end{bmatrix} = J^2 \tag{3.25}$$

where we have expressed $\mathbf{R}$ in it's cartesian components, and where $\det(\mathbf{J}) = J$. Denoting the determinant of the covariant metric as $\det(g) = g$ we have the relation

$$\sqrt{g} = J \tag{3.26}$$

3.3 Differential operators in curvilinear geometry

With the metric and jacobian defined we now state the differential operators in curvilinear geometry. They are [12]:

The gradient:

$$\nabla \phi = \frac{\partial \phi}{\partial u^i} \nabla u^i \tag{3.27}$$

The divergence:

$$\nabla \cdot \mathbf{A} = \frac{1}{J} \frac{\partial}{\partial u^i} (J A^i) \tag{3.28}$$

The laplacian:

$$\nabla^2 \phi = \frac{1}{J} \frac{\partial}{\partial u^i} (J g^{ij}) \frac{\partial \phi}{\partial u^i} + g^{ij} \frac{\partial^2 \phi}{\partial u^i \partial u^j} \tag{3.29}$$

We now define a reference vector [12]

$$\mathbf{B}_0 = \nabla z \times \nabla x, B_0 = \frac{\sqrt{g_{yy}}}{J} \tag{3.30}$$

and

$$\mathbf{b}_0 = \frac{\mathbf{B}_0}{B_0} \tag{3.31}$$

The operators parallel and perpendicular to the magnetic field can now be defined.

We have the parallel gradient

$$\nabla_{\|} f = \mathbf{b}_0 \cdot \nabla f = \frac{1}{\sqrt{g_{yy}}} \frac{\partial}{\partial y} f \tag{3.32}$$

the parallel divergence

$$\nabla_{\|} \cdot \mathbf{f} = \frac{B_0}{\sqrt{g_{yy}}} \frac{\partial}{\partial y} \left(\frac{\mathbf{f}}{B_0} \right) \tag{3.33}$$

and the parallel laplacian

$$\nabla_{\|}^2 \phi = \nabla \cdot \mathbf{b}_0 \mathbf{b}_0 \cdot \nabla \phi = \frac{1}{J} \frac{\partial}{\partial y} \left(\frac{J}{g_{yy}} \frac{\partial \phi}{\partial y} \right) \tag{3.34}$$

With the differential operators defined in a general curvilinear coordinate system we are able to move on to describing the magnetic field.

Chapter 4

Field aligned coordinates

In order to reduce the computational cost of 3D fusion plasma models significantly, and due to the fact that the magnetic field plays a significant role in the confinement of the plasma, it is convenient to align the coordinates with the magnetic field. The computational time is reduced due to the particles moving rather freely along the magnetic field lines giving flat gradients in the fieldline direction. Furthermore the global shape of the magnetic field plays a significant role in the dynamics of the confined plasma, so an accurate description of the shape of the magnetic field is necessary for a realistic description of plasma dynamics.

In this section we will use the differential geometry introduced in chapter 3 to derive field-aligned coordinates, and to derive the metric for the field-aligned coordinates containing all necesarry information about the shape of the magnetic field.

4.1 The shape of the Magnetic Field

In this section we will describe the shape of the magnetic field in a tokamak.

Since the goal of this thesis is to simulate dynamics in a tokamak, the magnetic field of interest is axisymmetric meaning that the components of the magnetic field, when expressed in cylindrical coordinates (R, ϕ, z), are all independent of ϕ. Note that seen from above ϕ points in the clockwise direction [11], and not counterclockwise as in traditional cylindrical coordinates, meaning that $\hat{R} \times \hat{z} = \hat{\phi}$. The magnetic field is divergence free and can be written in terms of the vector potential $\mathbf{A}$ as $\mathbf{B} = \nabla \times \mathbf{A}$.

We can split the magnetic field of a tokamak into a toroidal part, described by $\hat{\phi}$, and a poloidal part, described by $\hat{z}$ and $\hat{R}$, such that

$$\mathbf{B} = \hat{R}B_R + \hat{z}B_z + \hat{\phi}B_\phi \tag{4.1}$$

The poloidal part can be rewritten, using the vector potential and the axisymmetric property of the magnetic field, as

$$B_p = \hat{R}\frac{\partial A_\phi}{\partial z} - \hat{z}\frac{1}{R}\frac{\partial (RA_\phi)}{\partial R} \tag{4.2}$$

To rewrite the magnetic field further, we introduce the poloidal flux function [11],

$$\psi(R, z) = -RA_\phi(R, z) \tag{4.3}$$

and rewrite the magnetic field in the poloidal direction to

$$B_p = \nabla\phi \times \nabla\psi \tag{4.4}$$

It is seen that $\mathbf{B} \cdot \nabla\psi = 0$, since

$$\mathbf{B} \cdot \nabla\psi = \mathbf{B} \cdot \left(\frac{\partial \psi}{\partial R}\hat{R} + \frac{\partial \psi}{\partial z}\hat{z} \right) = \frac{1}{R}\frac{\partial \psi}{\partial z}\frac{\partial \psi}{\partial R} - \frac{1}{R}\frac{\partial \psi}{\partial z}\frac{\partial \psi}{\partial R} = 0 \tag{4.5}$$

So the magnetic field lies on surfaces of constant ψ, which are called flux surfaces [11].

The toroidal component of the magnetic field is in the direction of ϕ, so we can write

$$B_t = \hat{\phi}B_\phi = I(\psi)\nabla\phi \tag{4.6}$$

where I is an arbitrary flux function [11]. The total magnetic field is then given by

$$\mathbf{B} = I(\psi)\nabla\phi + \nabla\phi \times \nabla\psi \tag{4.7}$$

4.1.1 MHD equilibrium

In order to find an expression for the poloidal flux function we must investigate magnetohydrodynamic equilibrium (MHD). The MHD equations are a special case of the Two-Fluid equations, where the fluid is modeled such that it consists of only one particle specie. A detailed derivation of MHD can be seen in books such as [9] and [6].

In order to investigate the MHD equilibrium, we start by defining some new quantities. We define the current density [11]

$$\mathbf{J} = \sum_{\sigma} n_\sigma q_\sigma \mathbf{u}_\sigma \tag{4.8}$$

where $\sum_\sigma$ denotes the sum over all species. The center of mass velocity [11]

$$\mathbf{U} = \frac{1}{\rho} \sum_{\sigma} m_\sigma n_\sigma \mathbf{u}_\sigma, \tag{4.9}$$

where

$$\rho = \sum_{\sigma} m_\sigma n_\sigma, \tag{4.10}$$

and finally the MHD scalar pressure [11]

$$p_{MHD} = \sum_{\sigma} P_\sigma \tag{4.11}$$

We now sum eq. (2.39) with respect to the two species of the two-fluid equation (the two species being electrons and ions), eq. (2.39), in order to get the MHD momentum equation

$$\rho \frac{d}{dt} \mathbf{U} = (\sum_{\sigma} n_\sigma q_\sigma) \mathbf{E} + \mathbf{J} \times \mathbf{B} - \nabla p_{MHD} \tag{4.12}$$

In MHD we look at spacial scales much larger than the debye length. The debye length is the average length scale at which a charged particles charge is cancelled by surrounding particle charges. Looking at scales much larger than the debye length means we have quasineutrality and no charge effects are seen on these length scales, and thus $(\sum_\sigma n_\sigma q_\sigma)\mathbf{E} \approx 0$. Furthermore looking at static equilbria we have [11]

$$\mathbf{J} \times \mathbf{B} = \nabla p_{MHD}. \tag{4.13}$$

Using the axisymmetric representation of the magnetic field given by eq. (4.7), and the MHD equilibrium equation given by, eq. (4.13) we get

$$I(\psi)\mathbf{J} \times \nabla\phi + (\mathbf{J} \cdot \nabla\psi)\nabla\phi - (\mathbf{J} \cdot \nabla\phi)\nabla\psi = \nabla p_{MHD}. \tag{4.14}$$

This can be dotted with $\nabla\psi$ on both sides to give

$$(I(\psi)\mathbf{J} \times \nabla\phi - (\mathbf{J} \cdot \nabla\phi)\nabla\psi) \cdot \nabla\psi = \nabla p_{MHD} \cdot \nabla\psi \tag{4.15}$$

Using Amperes law for a static electric field

$$\nabla \times \mathbf{B} = \mu_0 \mathbf{J} \tag{4.16}$$

and plugging in the expression for the magnetic field (eq. (4.7)) we get

$$\mu_0\mathbf{J} = \nabla \times (I(\psi)\nabla\phi + \nabla\phi \times \nabla\psi) \tag{4.17}$$
$$= \nabla I(\psi) \times \nabla\phi + \nabla^2\psi\nabla\phi + (\nabla\psi \cdot \nabla)\nabla\phi \tag{4.18}$$

From eq. (4.13) it is clear that the magnetic field and the current density lies on surfaces of constant ∇p_{MHD}, due to the fact that $\mathbf{B} \cdot \nabla p_{MHD} = \mathbf{J} \cdot \nabla p_{MHD} = 0$. This implies that the pressure is a flux function [11]. The poloidal part of eq. (4.18) is

$$\mu_0\mathbf{J}_p = \nabla I \times \nabla\phi \tag{4.19}$$

since $\nabla\phi$ is in the toroidal direction. We can now calculate the toroidal part of the current by plugging the poloidal part into eq. (4.15)

$$(\mu_0^{-1} I(\nabla I \times \nabla\phi) \times \nabla\phi - (\mathbf{J}\cdot\nabla\phi)\nabla\psi)\cdot\nabla\psi = \nabla p_{MHD}\cdot\nabla\psi \tag{4.20}$$

where

$$\mu_0^{-1} I(\nabla I \times \nabla\phi) \times \nabla\phi = \mu_0^{-1} I(\nabla I\cdot\nabla\phi)\nabla\phi - \mu_0^{-1} I(\nabla\phi\cdot\nabla\phi)\nabla I \tag{4.21}$$

$$= -\mu_0^{-1} I\left(\frac{1}{R^2}\right)\nabla I \tag{4.22}$$

where we have used that $\nabla\phi\cdot\nabla\phi = g^{\phi\phi} = \frac{1}{R^2}$[1]. Using the chain rule, such that $\nabla I = \frac{\partial}{\partial\psi} I\nabla\psi$ and $\nabla p_{MHD} = \frac{\partial}{\partial\psi} p_{MHD}\nabla\psi$ and denoting the partial derivative with respect to ψ by $'$ we have

$$\left(\frac{II'}{\mu_0 R^2} - \mathbf{J}\cdot\nabla\phi\right) g^{\psi\psi} = p'_{MHD} g^{\psi\psi} \Rightarrow \tag{4.23}$$

$$\mathbf{J}\cdot\nabla\phi = -(p'_{MHD} + \frac{II'}{\mu_0 R^2}) \tag{4.24}$$

We now plug in our result in to the poloidal part of eq. (4.18)

$$(\nabla\times\mathbf{B})\cdot\nabla\phi = -\mu_0\left(p'_{MHD} + \frac{II'}{\mu_0 R^2}\right) \tag{4.25}$$

Using a vector rule, we rewrite $(\nabla\times\mathbf{B})\cdot\nabla\phi = \mathbf{B}\cdot(\nabla\times\nabla\phi) + \nabla\cdot(\mathbf{B}\times\nabla\phi)$. Using the expression for the magnetic field given in eq. (4.7) and the fact that the curl of a gradient is zero we have

$$\nabla\cdot(\mathbf{B}\times\nabla\phi) = \nabla\cdot((I\nabla\phi + \nabla\phi\times\nabla\psi)\times\nabla\phi) \tag{4.26}$$

$$= \nabla\cdot((\nabla\phi\times\nabla\psi)\times\nabla\phi) \tag{4.27}$$

$$= \nabla\cdot\left(\frac{1}{R^2}\nabla\psi\right) \tag{4.28}$$

[1] See Appendix A for the derivation of toroidal metric components

where we have once again used that $g^{\phi\phi} = \nabla\phi \cdot \nabla\phi = \frac{1}{R^2}$. Plugging this in to eq. (4.25) and multiplying by R^2 on both sides gives

$$R^2\nabla \cdot \left(\frac{1}{R^2}\nabla\psi\right) = -\mu_0 R^2 p'_{MHD} - II' \tag{4.29}$$

Eq. (4.29) is called the Grad-Shafranov equation, and the solutions to it describes the possible plasma equilibria [11]. In the general case eq. (4.29) is only solveable numerically. We will, however, use an approximate analytical solution, called the circle equilibrium solution later on as a basis for our numerical investigation.

4.2 Modified Hamada coordinates

In order to align the coordinates with the magnetic field, an intermediate step is to create a set of what is called flux coordinates. Flux coordinates are created in a way, such that the coordinate system consists of two angular (or angle like) coordinates and a radial flux coordinate which is defined to be constant on a given flux surface [10].

For our flux coordinate we simply choose the poloidal flux function given in eq. (4.3). For the other coordinates we impose that the contravariant components of the magnetic field in our coordinate system are flux functions [13] . We can then write the contravariant components of the magnetic field as:

$$B^\psi = \mathbf{B} \cdot \nabla\psi = 0 \tag{4.30}$$
$$B^\theta = \mathbf{B} \cdot \nabla\theta = \chi'(\psi) \tag{4.31}$$
$$B^\zeta = \mathbf{B} \cdot \nabla\zeta = \upsilon'(\psi) \tag{4.32}$$

In order to proceed we must derive the two angle coordinates, by requiring that the gradient of the coordinate dotted with the magnetic field must be flux functions.

We start by deriving an expression for the poloidal-like coordinate θ. For this, we start by introducing a parametric coordinate η defined in a way such that it is monotonically increasing along the flux surface in the poloidal direction [13]. It can hence be viewed as a coordinate describing the position along the magnetic field line in the poloidal plane. This implies that $\nabla\eta \perp \nabla\phi$. We can now express θ in terms of the coordinates r, η, ϕ, where r, η can be found from a one-to-one mapping from the poloidal part of the cylindrical coordinates $R, z \to r, \eta$. Now using the chain rule we have

$$\mathbf{B} \cdot \nabla\theta = \mathbf{B} \cdot \nabla\eta \frac{\partial\theta}{\partial\eta} + \mathbf{B} \cdot \nabla\phi \frac{\partial\theta}{\partial\phi} + \mathbf{B} \cdot \nabla r \frac{\partial\theta}{\partial r} \tag{4.33}$$

$$= \mathbf{B} \cdot \nabla\eta \frac{\partial\theta}{\partial\eta}. \tag{4.34}$$

Note that going from eq. (4.33) to (4.34) is only approximately true, it can, however, be shown by solving the Grad-Shafranov equation that $\mathbf{B} \cdot \nabla r$ is neglegible [13].

By seperating variables and using the contravariant θ-component of the magnetic field given by eq. (4.31) we have

$$\partial\theta = \chi'(\psi) \frac{\partial\eta}{\mathbf{B} \cdot \nabla\eta} \Rightarrow \tag{4.35}$$

$$\theta = \chi'(\psi) \int_{\eta_0}^{\eta} \frac{d\eta}{\mathbf{B} \cdot \nabla\eta} \tag{4.36}$$

where we have defined

$$\chi'(\psi) = 2\pi \left(\oint \frac{d\eta}{\mathbf{B} \cdot \nabla\eta} \right)^{-1} \tag{4.37}$$

in order for θ to be periodic in 2π [13]. We now have a coordinate θ that ensures a contravariant component of B^θ which is a flux function.

For the other angle-like coordinate we can not simply choose the toroidal coordinate as before, since

$$B^\phi = \mathbf{B} \cdot \nabla\phi = I g^{\phi\phi} = \frac{I}{R^2} \tag{4.38}$$

is not a flux function[2]. We can, however, choose the toroidal coordinate plus a function and require that the sum of the two components of the contravariant part of the magnetic field is a flux function. We then define the ζ-coordinate to be [13]

[2]While I is indeed a flux function, the same is not true for $\frac{1}{R^2}$ in general.

$$\zeta = \phi + f(\eta, \psi) \tag{4.39}$$

which, with our requirements, gives

$$\mathbf{B} \cdot \nabla\zeta = \frac{\partial \zeta}{\partial \phi}\mathbf{B} \cdot \nabla\phi + \frac{\partial \zeta}{\partial \eta}\mathbf{B} \cdot \nabla\eta \tag{4.40}$$

$$= \frac{I}{R^2} + \mathbf{B} \cdot \nabla\eta \frac{\partial f}{\partial \eta} = \upsilon'(\psi) \tag{4.41}$$

This leaves us with an equation for f

$$f = \int_{\eta_0}^{\eta} \frac{d\eta}{\mathbf{B} \cdot \nabla\eta}\left(\upsilon'(\psi) - \frac{I}{R^2}\right) \tag{4.42}$$

We now require that over a flux surface average we move in the ϕ-direction [13]. We start by defining the general flux surface average

$$\langle h(\eta, \psi) \rangle = \frac{\chi'}{2\pi} \int_{\eta_0}^{\eta^1} \frac{d\eta}{\mathbf{B} \cdot \nabla\eta} h(\eta, \psi) \tag{4.43}$$

where in the case of closed flux surfaces we have $\eta_0 = 0$ and $\eta_1 = 2\pi$. Now, since we require that the flux surface average of f dissappears, we must have

$$\upsilon'(\psi) = \left\langle \frac{I(\psi)}{R^2} \right\rangle = I \left\langle \frac{1}{R^2} \right\rangle \tag{4.44}$$

For the last coordinate we then get

$$\zeta = \phi + I \int_{\eta_0}^{\eta} \frac{d\eta}{\mathbf{B} \cdot \nabla\eta}\left(\left\langle \frac{1}{R^2} \right\rangle - \frac{1}{R^2}\right) \tag{4.45}$$

The derived coordinate system, also called modified Hamada coordinates[3], preserves the axisymmetry [13], but is no longer orthogonal, which can be seen by the fact that the contravariant metric has non-diagonal components[4]. We have also ensured a periodicity in θ and ζ.

[3]These Coordinates differ from the usual Hamada coordinates by not requiring that the Jacobian is one. [10] [13]

[4]Since this is equivalent to the fact that $\nabla x^i \cdot \nabla x^j$ is not zero for all $i \neq j$

4.3 Field-Aligned Hamada Coordinates

We now go back to looking at the magnetic field. The goal is to have the contravariant component of the magnetic field be zero in all, except for one coordinate, denoted as y, since this is equivalent to the magnetic field moving along the ∇y.

As expressed by eqns. (4.30)-(4.32) we know that we must be able to express the magnetic field in terms of a cross product between $\nabla\psi$ and something else. Now using the inverse of eqns (3.13)-(3.15) and eq. (3.19) we can write

$$\begin{aligned}\mathbf{B} &= (\mathbf{B}\cdot\nabla\psi)\mathbf{e}_\psi + (\mathbf{B}\cdot\nabla\theta)\mathbf{e}_\theta + (\mathbf{B}\cdot\nabla\zeta)\mathbf{e}_\zeta && (4.46)\\ &= \frac{\chi'\nabla\zeta\times\nabla\psi + \upsilon'\nabla\psi\times\nabla\zeta}{\nabla\psi\cdot(\nabla\theta\times\nabla\zeta)} && (4.47)\\ &= J\nabla\psi\times(\upsilon'\nabla\theta - \chi'\nabla\zeta) && (4.48)\end{aligned}$$

where $\frac{1}{\nabla\psi\cdot(\nabla\theta\times\nabla\zeta)}$ is the same as the Jacobian of the covariant metric of the coordinate system [10]. Now the safety factor, the number of full toroidal circuits per full poloidal circuits of a magnetic field line, can be expressed as

$$q(\psi) = \frac{\langle\mathbf{B}\cdot\nabla\phi\rangle}{\langle\mathbf{B}\cdot\nabla\theta\rangle} = \frac{\mathbf{B}\cdot\zeta}{\mathbf{B}\cdot\theta} = \frac{\chi'}{\upsilon'} \tag{4.49}$$

which means we can rewrite the expression for the magnetic field to [13]

$$\mathbf{B} = \chi' J\nabla(\zeta - q\theta)\times\nabla\psi \tag{4.50}$$

We can now create a coordinate system aligned with the magnetic field. A naive guess would be to choose our new coordinates such that they read

$$\begin{aligned}x' &= \psi && (4.51)\\ y' &= \theta && (4.52)\\ z' &= \zeta - q\theta, && (4.53)\end{aligned}$$

however, in the programming platform/C++ package manager used in this thesis called BOUT++ [14], it is more convenient to have the magnetic field written in what is called normalized Clebsch form [10]. Normalized Clebsch form means that the magnetic field is represented as [10]

$$\mathbf{B} = \mathbf{e}^3 \times \mathbf{e}^1 \tag{4.54}$$

We know that χ' is a flux function and the Jacobian is also a flux function [13]. This can be shown by requiring that the magnetic field be divergence free (which it must be according to Maxwells equations), and by taking the divergence of eq. (4.48), and using several vector rules[5] and the fact that χ' and υ' are flux functions we have [13]

$$\nabla \cdot \mathbf{B} = \nabla J \cdot \nabla\psi \times (\upsilon' \nabla\theta - \chi' \nabla\zeta) = 0 \tag{4.55}$$

which means that $J \parallel \psi$, and thus that J is a flux function. This allows us to define a coordinate that is a flux function, and write the magnetic field on normalized Clebsch form. The coordinates are

$$x = \int (J\chi') d\psi \tag{4.56}$$

$$y = \theta \tag{4.57}$$

$$z = \zeta - q\theta \tag{4.58}$$

and the magnetic field is

$$\mathbf{B} = \nabla z \times \nabla x \tag{4.59}$$

Note that the shift in z makes y aligned with the magnetic field. This can be explained by holding z constant and moving along y, if you do so you must move along both θ and ζ. Where the Hamada coordinates were periodic, this is no longer the case for the y-coordinate. However we do have what is called pseudoperiodicity, which means that

$$f(x, y + 2\pi, z) = f(x, y, z - 2\pi q) \tag{4.60}$$

We now have a set of field-aligned coordinates true for any solution to the Grad-Shafranov equation (eq. (4.29)).

[5] See Appendix B for useful vector identities

4.4 The Circle Equilibrium Model

In the simulations performed in this thesis a simple analytical solution to the Grad-Shafranov equation (eq. (4.29)) is used. In order to get an analytical expression for the fieldaligned coordinates and create a simple, but realistic model, a circle equilibrium solution to the Grad-Shafranov equation is assumed, which holds in the large aspect ratio limit, where $\frac{R_0}{r} >> 1$ (see figure 4.1). This assumption means that ψ is now a function of r only, where ϵ is the inverse aspect ratio $\frac{r}{R_0}$ and is a small parameter [11][6]. This inconsistency can be solved in future models involving more complex solutions to the Grad-Shafranov equation, but is not done in this thesis. The circle equilibrium model means that the parametric coordinate η reduces to the poloidal angle coordinate in a toroidal coordinate system[7]. We then have

$$\mathbf{B} \cdot \nabla\eta = (I\nabla\phi + \nabla\phi \times \nabla\psi) \cdot \nabla\eta = \frac{\partial\psi}{\partial r}\nabla\phi \times \nabla r \cdot \nabla\eta \tag{4.61}$$

$$= \frac{1}{J}\frac{\partial\psi}{\partial r} = \frac{1}{rR}\frac{\partial\psi}{\partial r} \tag{4.62}$$

where J is the Jacobian of a toroidal coordinate system, r denotes the minor radius and R denotes the major radius as seen on figure 4.1 [15].

From now on we denote the poloidal angle by η, since the poloidal angle is now equal to the parametric coordinate defined in the previous section. By calculating the safety factor q, we can get an expression for $\frac{\partial\psi}{\partial r}$.

$$q = \frac{\langle \mathbf{B} \cdot \nabla\phi \rangle}{\langle \mathbf{B} \cdot \nabla\eta \rangle} = \frac{\langle \frac{I}{R^2} \rangle}{\langle \frac{1}{rR}\psi' \rangle}. \tag{4.63}$$

Calculating the flux surface average of $\mathbf{B} \cdot \nabla\phi$ gives [13]

[6] Such a circle equilibrium can be found by assuming Solovev type solustions (where I is constant and $p_{MHD} \propto \psi$) to the Grad-Shafranov equation and using the large-aspect ratio limit [11]. Note that this is equivalent to throwing away terms of order $O(\epsilon)$ in the solution to the Grad-Shafranov equation whilst keeping terms of $O(\epsilon)$ in the other derivations [11]

[7] See Appendix A for a derivation of the toroidal coordinates, the metric entries and the Jacobian

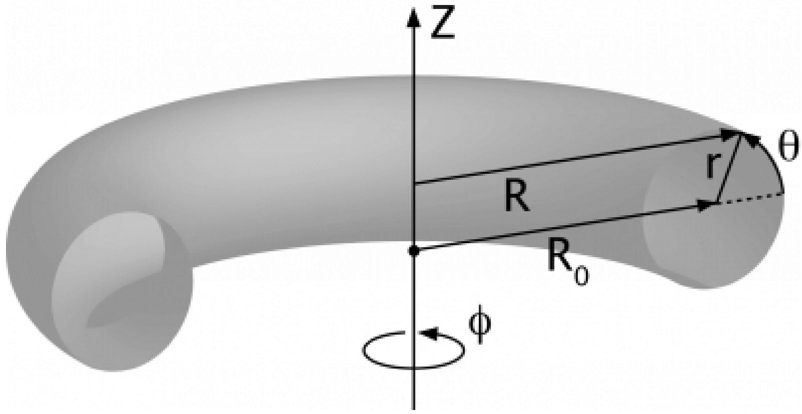

Figure 4.1: Toroidal coordinates (note that θ is different from the Hamada θ)

$$\langle \mathbf{B}\cdot\nabla\phi\rangle = \frac{\chi'}{2\pi}\int_0^{2\pi}\frac{I}{R^2}\frac{d\eta}{\mathbf{B}\cdot\nabla\eta} = \frac{r\chi' I}{R_0\psi' 2\pi}\int_0^{2\pi}\frac{1}{1+\epsilon\cos(\eta)} \tag{4.64}$$

$$= \frac{r\chi' I}{R_0\psi' 2\pi}\frac{2\pi}{\sqrt{1-\epsilon^2}}. \tag{4.65}$$

The flux surface average of $\mathbf{B}\cdot\nabla\eta$ is

$$\langle \mathbf{B}\cdot\nabla\eta\rangle = \frac{\chi'}{2\pi}\int_0^{2\pi} d\eta = \chi' \tag{4.66}$$

We now have an expression for q in terms of flux functions only,

$$q = \frac{rI}{R_0\psi'\sqrt{1-\epsilon^2}}, \tag{4.67}$$

which gives us an expression for ψ'

$$\psi' = \frac{rI}{R_0 q\sqrt{1-\epsilon^2}} \tag{4.68}$$

We now calculate the angle-like Hamada coordinates for the circle equilibrium model. Recalling eq. (4.36) all we have to calculate is the integral. We have

$$\int_{\eta_0}^{\eta} \frac{d\eta}{\mathbf{B}\cdot\nabla\eta} = \frac{r}{\psi'}\int_{\eta_0}^{\eta} R_0(1+\epsilon\cos(\eta))d\eta = \frac{rR_0}{\psi'}[\eta+\epsilon\sin(\eta)]_{\eta_0}^{\eta} \tag{4.69}$$

From eq. (4.37) we have the definition of χ', which in our case leads to

$$\chi' = \frac{\psi'}{rR_0} \tag{4.70}$$

so our theta coordinate (eq. (4.36)) becomes

$$\theta = [\eta+\epsilon\sin(\eta)]_{\eta_0}^{\eta} \tag{4.71}$$

From eq. (4.45) we have an expression for the ζ-coordinate, which involves two integrals. We start by calculating the flux-surface averaged part.

$$\left\langle \frac{1}{R^2} \right\rangle = \frac{r\chi'}{2\pi\psi'}\int_0^{2\pi} \frac{d\eta}{R_0(1+\epsilon\cos(\eta))} = \frac{r\chi'}{2\pi R_0\psi'}\frac{2\pi}{\sqrt{1-\epsilon^2}} = \frac{1}{R_0^2\sqrt{1-\epsilon^2}} \tag{4.72}$$

The first integral can then be found by multiplying the flux average of $\frac{1}{R^2}$ by eq. (4.69). The second integral gives us

$$\int_{\eta_0}^{\eta} \frac{1}{R^2}\frac{d\eta}{\mathbf{B}\cdot\nabla\eta} = \frac{r}{R_0\psi'}\int_{\eta_0}^{\eta}\frac{d\eta}{1+\cos(\eta)} \tag{4.73}$$

Here one has to be careful when solving the definite integral, since it is not possible to solve the indefinite integral and put in the limits, due to discontinuities in the solution to the indefinite integral. However in the simulations we only look at the limit between $-\pi+\delta$ and $\pi-\delta$ where the discontinuities are not present, in which case the solution to the integral above becomes

$$\int_{\eta_0}^{\eta} \frac{1}{R^2} \frac{d\eta}{\mathbf{B} \cdot \nabla \eta} = \frac{r}{R_0 \psi'} \left[2 \frac{\arctan\left(\sqrt{\frac{1-\epsilon}{1+\epsilon}} \tan(\frac{\eta}{2})\right)}{\sqrt{1-\epsilon^2}} \right]_{\eta_0}^{\eta} \tag{4.74}$$

which leads to a new expression for ζ,

$$\zeta = \phi + \frac{Ir}{\psi' R_0 \sqrt{1-\epsilon^2}} ([\eta + \epsilon \sin(\eta)]_{\eta_0}^{\eta} - [2 \arctan(\sqrt{\frac{1-\epsilon}{1+\epsilon}} \tan(\frac{\eta}{2}))]_{\eta_0}^{\eta}) \tag{4.75}$$

$$= \phi + q \left([\eta + \epsilon \sin(\eta)]_{\eta_0}^{\eta} - \left[2 \arctan\left(\sqrt{\frac{1-\epsilon}{1+\epsilon}} \tan(\frac{\eta}{2}) \right) \right]_{\eta_0}^{\eta} \right) \tag{4.76}$$

Note that this does not look periodic in 2π in η. That is, however, because the definite integral from 0 to 2π is not found by evaluating the indefinite integral in the limits, and when evaluating the definite integral from 0 to 2π one finds, that it is in fact periodic.

4.4.1 The Contravariant Hamada Metric

We now move on to calculating the Hamada metric before calculating the field aligned metric.

In order to calculate the contravariant metric elements of the Hamada coordinates we must first calculate the gradients of the respective coordinates. Since we work in a circle equilibrium we have, by using the chain rule,

$$\nabla x = J\chi' \nabla \psi = J\chi' \psi' \nabla r \tag{4.77}$$

In this section we will be calculating the metric where we use r as the first coordinate instead of ψ, since later inclusion of the $J\chi'\psi'$ prefactors when calculating the field aligned metric is trivial.

For the first angle-like coordinate we get

$$\nabla \theta = \nabla \eta + \epsilon \cos(\eta) \nabla \eta + \frac{1}{R_0} \sin(\eta) \nabla r \tag{4.78}$$

For the second angle-like coordinate we define a function

$$f = 2\arctan\left(\sqrt{\frac{1-\epsilon}{1+\epsilon}}\tan\left(\frac{\eta}{2}\right)\right)$$

for simplicity. This gives

$$\nabla\zeta = \nabla\phi - \left(q\frac{\partial}{\partial r}f + f\frac{\partial}{\partial r}q - \eta\frac{\partial}{\partial r}q - \frac{\partial}{\partial r}(q\epsilon)\sin(\eta)\right)\nabla r \\ - \left(q\frac{\partial}{\partial \eta}f - (1+\epsilon\cos(\eta))\right)\nabla\eta \tag{4.79}$$

It can be shown that the contravariant metric coefficients for a torus are (see Appendix A for derivation)

$$g^{rr} = 1 \tag{4.80}$$

$$g^{\eta\eta} = \frac{1}{r^2} \tag{4.81}$$

$$g^{\phi\phi} = \frac{1}{R^2} \tag{4.82}$$

where $R = R_0 + r\cos(\eta)$, and all the off-diagonal metric components are zero. We now derive the contravariant Hamada metric coefficients:

$$g^{rr} = \nabla r \cdot \nabla r = 1 \tag{4.83}$$

$$g^{\theta\theta} = \nabla\theta \cdot \nabla\theta = (1 + \epsilon\cos(\eta))^2 \cdot \frac{1}{r^2} + \left(\frac{cos(\eta)}{R_0}\right)^2 \tag{4.84}$$

$$\begin{aligned} g^{\zeta\zeta} = \nabla\zeta \cdot \nabla\cdot = \frac{1}{R^2} &- \left(q\frac{\partial}{\partial r}f + f\frac{\partial}{\partial r}q - \eta\frac{\partial}{\partial r}q - \sin(\eta)\frac{\partial}{\partial r}(q\epsilon)\right)^2 \\ &- \left(q\frac{\partial}{\partial \eta}f - (1 + \epsilon\cos(\eta))\right)^2 \cdot \frac{1}{r^2} \end{aligned} \tag{4.85}$$

$$g^{r\theta} = \nabla r \cdot \nabla\theta = \frac{\cos(\eta)}{R_0} \tag{4.86}$$

$$g^{r\zeta} = \nabla r \cdot \nabla\zeta = \eta\frac{\partial}{\partial r}q + \sin(\eta)\frac{\partial}{\partial r}(q\epsilon) - q\frac{\partial}{\partial r}f - f\frac{\partial}{\partial r}q \tag{4.87}$$

$$\begin{aligned} g^{\theta\zeta} = \nabla\theta \cdot \nabla\zeta = -\frac{1}{R_0}\cos(\eta) \cdot (q\frac{\partial}{\partial r}f + f\frac{\partial}{\partial r}q - \eta\frac{\partial}{\partial r}q - \frac{\partial}{\partial r}(q\epsilon)\sin(\eta)) \\ - \frac{1}{r^2}(1 + \epsilon\cos(\eta))(q\frac{\partial}{\partial \eta}f - (1 + \epsilon\cos(\eta))) \end{aligned} \tag{4.88}$$

Note that $g^{\zeta\zeta}$,$g^{r\zeta}$ and $g^{\theta\zeta}$ are not periodic with respect to the poloidal angle, however this is again because the calculated metric elements only hold in the range $]-\pi, \pi[$. We now have the contravariant Hamada metric which will be a help when deriving the field-aligned contravariant Hamada metric.

4.4.2 The Contravariant Field-Aligned Hamada Metric

In the same way as we calculated the contravariant Hamada metric coefficients we now calculate the conravariant metric for the field aligned coordinates.

The gradients of eqns. (4.56)-(4.58) are:

$$\nabla x = J\frac{\partial \chi}{\partial \psi}\frac{\partial \psi}{\partial r}\nabla r \tag{4.89}$$

$$\nabla y = \nabla \theta \tag{4.90}$$

$$\nabla z = \nabla \zeta - \theta\frac{\partial}{\partial r}q\nabla r - q\nabla\theta \tag{4.91}$$

where J denotes the Jacobian of the covariant Hamada metric (the real Hamada metric with the first coordinate being ψ). The Jacobian can be found by taking the square root of the inverse of the determinant of the contravariant Hamada metric and gives

$$J = \frac{rR_0}{\psi'} \tag{4.92}$$

which means that

$$\nabla x = \psi'\nabla r \tag{4.93}$$

From this we can calculate the contravariant metric for the field aligned Hamada coordinates.

$$g^{xx} = \left(\frac{\partial}{\partial r}\Psi\right)^2 \tag{4.94}$$

$$g^{yy} = g^{\theta\theta} \tag{4.95}$$

$$g^{zz} = \left(\theta\frac{\partial}{\partial r}q\right)^2 + q^2 g^{\theta\theta} + g^{\zeta\zeta} + 2q\theta\frac{\partial}{\partial r}qg^{r\theta} - 2\theta\frac{\partial}{\partial r}qg^{r\zeta} - 2qg^{\theta\zeta} \tag{4.96}$$

$$g^{xy} = \left(\frac{\partial}{\partial r}\Psi\right)g^{r\theta} \tag{4.97}$$

$$g^{xz} = \left(\frac{\partial}{\partial r}\Psi\right)\left(g^{r\zeta} - \theta\frac{\partial}{\partial r}qg^{rr} - qg^{r\theta}\right) \tag{4.98}$$

$$g^{yz} = g^{\theta\zeta} - \theta\left(\frac{\partial}{\partial r}q\right)g^{r\theta} - qg^{\theta\theta} \tag{4.99}$$

The Jacobian for the field aligned metric is the same as for the modified Hamada metric.

We now have the metric needed for simulations in field-aligned coordinates, which allows us to move on to deriving the modified Hasegawa-Wakatani equations in field aligned geometry.

Chapter 5

The Hasegawa-Wakatani Equations

We start this chapter by stating a number of assumptions used on the two-fluid equations in order to derive a simple set of equations for describing the evolution of a fusion plasma in three dimensions called the Hasegawa-Wakatani equations. Part of the solution to the Hasegawa-Wakatani equations gives rise to drift waves in the direction perpendicular to the magnetic field [16].

5.1 Assumptions

The assumptions are as follows [16, 17]:

Assumption 1 $\frac{T_i}{T_e} \ll 1$

The ion temperature is much smaller than the electron temperature and can hence be neglected.

Assumption 2 $\beta = \frac{n_e T_e}{\frac{B^2}{2\mu_0}} \ll 1$

We assume that the magnetic field pressure is much larger than the particle pressure. The plasma is then said to be a low β-plasma.

Assumption 3 $\boldsymbol{E} = -\nabla\phi$

Pertubations in the density and potential of the plasma lead to pertubations in the magnetic field, however these pertubations are small, so we assume that we have a static magnetic field, and hence that the electric field is curl-free.

Assumption 4 $k^2 \ll \frac{1}{\lambda_D^2}$

where λ_D is the debye length[1]. We assume that the wave number for the drift waves is much larger than the inverse Debye length.

Assumption 5 $n_e = n_i = n$

Assumption 4 allows us to assume quasi-neutrality which means that the density of the electrons and ions is the same.

Assumption 6 $n = n_0 + n_1$

The density can be written in terms of a background density and a density pertubation, where n_0 is the background density and n_1 is the density pertubation.

Assumption 7 $n_0 = N_0 e^{-\frac{x}{L_n}}$

We assume that the background density is of the form $n_0 = N_0 e^{-\frac{x}{L_n}}$ in the edge regions of the plasma, where N_0 is a constant and L_n is a characteristic length scale for the density gradient.

Assumption 8 $\frac{n_1}{n_0} \sim \frac{e\phi}{T_e} \sim \frac{\omega}{\omega_{ci}} \ll 1$

The relative pertubations in the density, the potential and the ion vorticity are assumed to be small, where $\omega_{ci} = \frac{eB}{m_i}$ is the ion cyclotron frequency. This assumption means that

$$\ln(n) \approx \ln(n_0) + \frac{n_1}{n_0}$$

Assumption 9 $\omega_t \ll \omega_{ci}$

[1]The Debye length is the average length at which a particle in a plasma is "shielded", such that it's charge approximately cancels with the charges sorrounding it

Furthermore we assume that the drift wave frequency, ω_t, is much smaller than the gyrofrequency[2] and that the dominant drift perpendicular to the magnetic field is the $\mathbf{E} \times \mathbf{B}$-drift and the diamagnetic drift, where the drift wave frequency is a typical timescale of turbulence.

Assumption 10 $k_{\|} \ll k_x \sim k_z$

We assume that the variation of the drift waves is mainly in the perpendicular direction.

Assumption 11 $P_\sigma = n_\sigma T_\sigma$,

where κ has been included in T_σ. The electrons and ions are assumed to be an isothermal fluid.

Assumption 12 $u_{i\|} = 0$

The fact that the ion mass is much larger than the electron mass allows us to assume that the ion inertia fixes the ions in the parallel direction, together with assumption 1 this leads to zero velocity for the ions in the direction of the magnetic field.

Assumption 13 $\frac{\nabla T_\sigma}{\nabla n_0} \ll 1$

Temperature gradient effects can be neglected.

Assumption 14 *The dominant drift is the 0th order drift*

We assume that the dominant drift in the perpendicular direction is the 0th order drift i.e. eq. (2.47).

Since we are working in field-aligned coordinates the magnetic field follows straight lines in the y-direction defined earlier. All differential vector operators in the following sections denote the operators in curvilinear geometry as defined in the last section of chapter 3.

[2]For a detailed description of typical plasma frequencies see books such as [9], [6] and [18]

5.2 The Electron Fluid

We now derive the Hasegawa-Wakatani equations in the field-aligned coordinates derived in chapter 4 using the above assumptions. We start by looking at the motion of the electron fluid.

In chapter 2 we derived the two-fluid equations and the fluid drift velocity in the perpendicular direction. The electron fluid has a velocity both parallel and perpendicular to the magnetic field, and we can split the velocity of the electrons in to two terms, such that $\mathbf{u}_e = \mathbf{u}_{e\perp} + u_{e\|}\mathbf{e}_y$. We now need an expression for the velocity in the direction parallel to the magnetic field. We recall eq. (4.8) defining the current

$$\mathbf{J} = \sum_\sigma n_\sigma q_\sigma \mathbf{u}_\sigma$$

Now if we take only the parallel component of the current, given by eq. (4.8), the expression reduces to

$$J_\| = -n_e e u_{e\|} \tag{5.1}$$

due to the neglection of ion velocity in the y-direction (assumption 12).

By now including the electron momentum equation, eq (2.39), and rewriting it by using the isothermal limit we have

$$n_e m_e \frac{d\mathbf{u}_e}{dt} = -n_e e(\mathbf{E} + \mathbf{u}_e \times \mathbf{B}) - \nabla n_e T_e - \nu_{ei} m_e n_e (\mathbf{u}_e - \mathbf{u}_i) \tag{5.2}$$

Due to assumption 9 the inertial term of the electron momentum equation can be neglected, which then leaves us with

$$E_\| = -\frac{1}{n_e e}\nabla_\| n_e T_e + \eta J_\| \tag{5.3}$$

where we have introduced the plasma resisitivity, $\eta = \frac{\nu_{ei} m_e}{n_e e^2}$. Now using assumption 3 and assumption 11 we can rewrite the parallel current as

$$J_\| = -\frac{T_e}{\eta e}\left(\frac{1}{n_e}\nabla_\| n_e - \nabla_\| \left(\frac{e\phi}{T_e}\right)\right) \tag{5.4}$$

Recalling eq. (2.47) we can now write the total flow velocity of the electron fluid[3]

$$\mathbf{u}_e = \frac{\mathbf{E}\times\mathbf{B}}{B^2} + \frac{\nabla P_\sigma \times \mathbf{B}}{n_e e B^2} - \frac{1}{n_e e} J_\parallel \tag{5.5}$$

Taking a look at the electron continuity equation we have, from eq. (2.38),

$$\frac{\partial n_e}{\partial t} + \nabla\cdot(n_e \mathbf{u}_e) = 0 \tag{5.6}$$

The dot product between the diamagnetic drift and the gradient of the density is zero due to assumption 13, and the divergence of the perpendicular drifts is zero, so the perpendicular part of the second term on the left hand side reads

$$\nabla\cdot(n_e \mathbf{u}_e)_\perp = \frac{\mathbf{E}\times\mathbf{B}}{B^2}\cdot\nabla n_e \tag{5.7}$$

The divergence of the parallel part is given by

$$\nabla_\parallel\cdot(n_e u_\parallel) = -\frac{1}{e}\nabla_\parallel\cdot J_\parallel \tag{5.8}$$

Rewriting the electron continuity equation and using quasi-neutrality we then have

$$\frac{\partial n}{\partial t} - \frac{\nabla\phi\times\mathbf{B}}{B^2}\cdot\nabla n = \frac{1}{e}\nabla_\parallel\cdot J_\parallel \tag{5.9}$$

defining the convective derivative in terms of the $\mathbf{E}\times\mathbf{B}$-drift as $\frac{D}{Dt} = \frac{\partial}{\partial t} + \mathbf{u}_E\cdot\nabla$, the expression is simplified to

$$\frac{D}{Dt}n = \frac{1}{e}\nabla_\parallel\cdot J_\parallel \tag{5.10}$$

This equation in combination with the expression for the parallel current is the first modified Hasegawa-Wakatani equation[4].

[3] The first order drift can be neglected for electrons due to $\omega_{ce} \gg \omega_{ci}$, however the ions have a larger mass than electrons

[4] Modified due to the fact that the original set of equations assume a slab coordinate system

5.3 The Ion Fluid

When finding the second equation of the Hasegawa-Wakatani model we utilize the assumption that the ions are cold, thus enabling us to neglect the diamagnetic drift and the drift parallel to the magnetic field. The only remaining 0th order drift is then the $\mathbf{E} \times \mathbf{B}$-drift. The first order drift for the ions is given by eq. (2.48) as

$$\mathbf{u}_i = -\frac{m_i}{eB^2}\left(\partial_t - \left(\frac{\nabla\phi \times \mathbf{B}}{B^2} \cdot \nabla\right)\right)\nabla\phi - \frac{\nabla\phi \times \mathbf{B}}{B^2} \tag{5.11}$$

Taking a look at the ion continuity equation, eq. (2.38), and plugging in the ion velocity we get

$$\begin{aligned} -\frac{1}{B\omega_{ci}}\left(\partial_t - \frac{\nabla\phi \times \mathbf{B}}{B^2} \cdot \nabla\right)\nabla^2\phi = \\ -\partial_t n + \left(\frac{\nabla\phi \times \mathbf{B}}{B^2} + \frac{1}{B\omega_{ci}}\left(\partial_t - \frac{\nabla\phi \times \mathbf{B}}{B^2} \cdot \nabla\right)\nabla\phi\right) \cdot \nabla n \end{aligned} \tag{5.12}$$

the $\frac{1}{B\omega_{ci}}\left(\partial_t - \frac{\nabla\phi\times\mathbf{B}}{B^2} \cdot \nabla\right)\nabla\phi$ term on the right hand side, also called the polariazation drift, is much smaller than the $\mathbf{E} \times \mathbf{B}$-drift due to assumption 14 and can be neglected. Introducing the convective derivative on both sides, and substituting eq. (5.10) in to the right hand side we get

$$\frac{D}{Dt}\frac{\nabla^2\phi}{B\omega_{ci}} = \frac{1}{en}\nabla_\parallel \cdot J_\parallel \tag{5.13}$$

This is the second Hasegawa-Wakatani equation. We now have a set of closed partial differential equations.

5.4 Normalizing the Hasegawa-Wakatani equations

When running simulations it is often convenient to normalize the equations. In order to normalize the Hasegawa-Wakatani equations, eq. (5.10) and eq.

(5.13), it is convenient to rewrite them. We start by using assumption 6 and using assumption 7 to rewrite the parallel current, eq. (5.4), to

$$J_{\|} = -\frac{T_e}{\eta e}\left(\nabla_{\|}\left(\ln(n_0) + \frac{n_1}{n_0}) - \nabla_{\|}(\frac{e\phi}{T_e}\right)\right) \tag{5.14}$$

where we have used $\nabla \ln(n) = \frac{1}{n}\nabla n$. Using assumption 8, the expression for the current simplifies to

$$J_{\|} = -\frac{T_e}{\eta e}\left(\nabla_{\|}\left(\frac{n_1}{n_0}\right) - \nabla_{\|}\left(\frac{e\phi}{T_e}\right)\right) \tag{5.15}$$

We now move on to rewriting the electron fluid eqaution (eq. (5.10)). Dividing eq. (5.10) by n on both sides gives

$$\frac{1}{n}\frac{D}{Dt}n = \frac{1}{ne}\nabla_{\|}J_{\|} \tag{5.16}$$

writing $n = n_0 + n_1$ and using once again that $\nabla \ln(n) = \frac{1}{n}\nabla n$ we have

$$\frac{D}{Dt}\ln(n_0 + n_1) = \frac{1}{e(n_0 + n_1)}\nabla_{\|}J_{\|} \tag{5.17}$$

using assumption 8 we can write

$$\frac{1}{en_0(1 + \frac{n_1}{n_0})} \approx \frac{1}{en_0} \tag{5.18}$$

and

$$\frac{D}{Dt}\left(\ln(n_0) + \frac{n_1}{n_0}\right) = \frac{1}{en_0}\nabla_{\|} \cdot J_{\|} \tag{5.19}$$

Eq. (5.13) can in the same way be rewritten to

$$\frac{D}{Dt}\frac{\nabla^2\phi}{B\omega_{ci}} = \frac{1}{en_0}\nabla_{\|} \cdot J_{\|} \tag{5.20}$$

Using the rewritten equations we now start the normalization. We introduce the normalized quantities

$$\tilde{l} = \frac{l}{\rho_s}, \tilde{t} = \omega_{ci} t, \tilde{\phi} = \frac{e\phi}{T_e}, \tilde{n} = \frac{n_1}{n_0}, \tilde{\nabla} = \rho_s \nabla$$

where l denotes any length parameter and $\rho_s = \frac{\sqrt{T_e m_i}}{eB}$ is the ion gyroradius at the electron temperature T_e. Plugging this in to the Hasegawa-Wakatani equations (eqns. (5.19) and (5.20)) and utilizing that $\partial_t n_0 = 0$ and adding a diffusion and viscosity term [17] to them, we end up with the normalized Hasegawa-Wakatani equations

$$(\tilde{\partial}_t + \tilde{\mathbf{u}}_E \cdot \tilde{\nabla})\tilde{n} + \tilde{\mathbf{u}}_E \cdot \tilde{\nabla}(\ln(n_0)) = \mathcal{C}\tilde{\nabla}_\parallel \cdot \tilde{\nabla}_\parallel(\tilde{n} - \tilde{\phi}) + \mu\tilde{\nabla}^2 n \tag{5.21}$$

$$(\tilde{\partial}_t + \tilde{\mathbf{u}}_E \cdot \tilde{\nabla})\tilde{\nabla}^2\tilde{\phi} = \mathcal{C}\tilde{\nabla}_\parallel \cdot \tilde{\nabla}_\parallel(\tilde{n} - \tilde{\phi}) + \mu\tilde{\nabla}^4 \tilde{\phi} \tag{5.22}$$

where

$$\mathcal{C} = \frac{T_e}{\eta e^2 n_0 \omega_{ci} \rho_s^2} \tag{5.23}$$

This normalization, however, also means that we must normalize the metric elements used in the differential operators. Utilizing that in the large aspect ratio limit we have $I \approx R_0 B_0$ [11,13], we have as an expression for ψ':

$$\psi' = \frac{r B_0}{q\sqrt{1-\epsilon^2}}. \tag{5.24}$$

The safety factor is unitless, and the SI units of ψ' is then tesla times metres. This leads to the normalization

$$g^{xx} = \nabla x \cdot \nabla x = \rho_s^2 B_0^2 \tilde{g}^{xx} \tag{5.25}$$

$$g^{yy} = \nabla y \cdot \nabla y = \frac{1}{\rho_s^2}\tilde{g}^{yy} \tag{5.26}$$

$$g^{zz} = \frac{1}{\rho_s^2}\tilde{g}^{zz} \tag{5.27}$$

$$g^{xy} = B_0 \tilde{g}^{xy} \tag{5.28}$$

$$g^{xz} = B_0 \tilde{g}^{xz} \tag{5.29}$$

$$g^{yz} = \frac{1}{\rho_s^2}\tilde{g}^{yz} \tag{5.30}$$

We now have a set of normalized, closed partial differential equations. The next step is to analyze the dynamics of the system described by the equations, and this is done by simulations using the BOUT++ platform.

Chapter 6

Simulations of the Hasegawa-Wakatani System

In this chapter we carry out simulations of the Hasegawa-Wakatani equations in our field-aligned system and define the numerical values for the field-aligned metric.

6.1 The Metric

The metric used in the simulations is the same as the circle equilibrium metric derived in chapter 4. We use the local approximation, which means that all r-dependencies are held constant while still including derivatives with respect to r, such that for instance $q(r) = Const$ and $\frac{\partial q}{\partial r} = Const \neq 0$. This leaves us with metric components that are only functions of the y-parameter.

In order to carry out the simulations we create a so-called grid file, which is a file including all necessary information about the coordinates. The spacing between each field-aligned coordinate and its neighbour is the same everywhere, which means the spacing is equidistant.[1]

In the metric there are several η-dependencies which we want expressed as funtions of y. However $y = \theta = \eta + \epsilon \sin(\eta)$, so finding an analytical expression for η in terms of y is not straightforward. This is solved by adding an iterative newton solver [19] in the grid file created. The solver finds the values of η for which $y - \eta - \epsilon \sin(\eta) = 0$ with equidistant gridspacing in y. In figure 6.1 we see how η is shifted with respect to θ when $\epsilon = 0.125$.

[1]For a detailed description of the finite difference methods used in BOUT++ see [12]

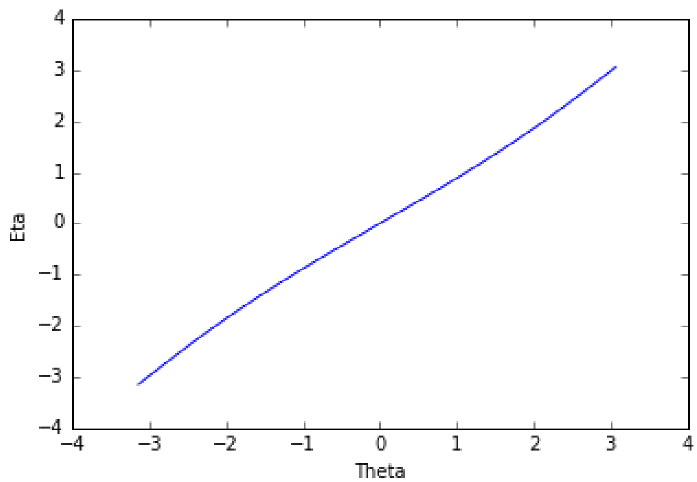

Figure 6.1: η plotted against θ

In our metric we assume $q(r)$ to be proportional to r^2, while requiring that q is still unitless.

For the simulations carried out in this chapter we have looked at a small Tokamak with a major radius of $R_0 = 1$ m and a minor radius of $r \approx 0.125$ m.

Table 6.1: Values for the metric

	symbol	value
Lowest value for the minor radius	r_{min}	0.1 m
Highest value for the minor radius	r_{max}	0.15 m
Average and assumed value for the minor radius	r_0	0.125 m
Major radius	R_0	1 m
The safety factor as a function of r	q	$2 + 7\frac{r}{R_0} + \frac{r^2}{R_0^2}$
The derivative of the safety factor with respect to r	q'	$\frac{7}{R_0} + 2\frac{r}{R_0^2}$

In table 6.1 all values used to derive the field-aligned metric used in the simulations performed in this chapter can be seen.

Plugging the values from table 6.1 into the metric elements of eqns.

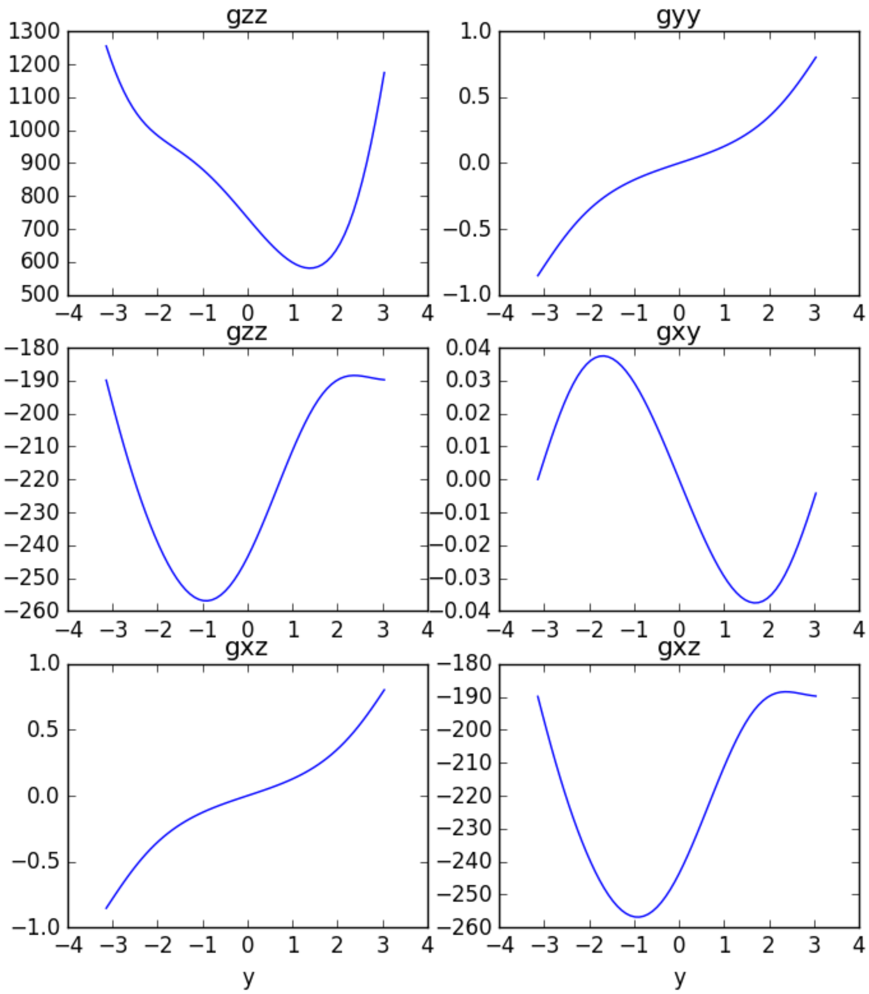

Figure 6.2: The metric coefficients of the field-aligned coordinates as functions of y

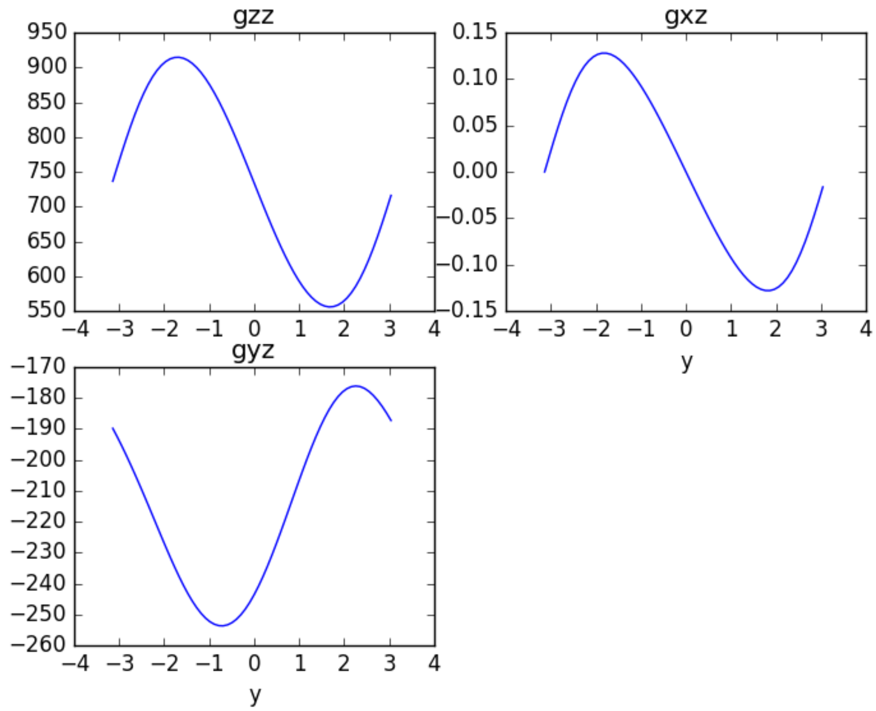

Figure 6.3: The metric coefficients depending on q' as functions of y

(4.94)-(4.99) gives figure 6.2. All the metric coefficients are shown as functions of y in the range $y =]-\pi, \pi[$. As seen, the metric elements containing z derivatives are not necessarily periodic nor continuous. The non-periodicity is due to the shift by $q\theta$ in the z-direction (eq. (4.58)) and the discontinuity is due to the discontinuous nature of the integral calculated for the ζ Hamada coordinate (eq. (4.74)). Furthermore note that the three z-dependent metric elements are highly dependent on the derivative of the safety factor with respect to r, in fact if we have $q' = 0$ all the metric elements end up periodic as seen in figure 6.3.

With our evaluation of the field-aligned metric complete we are now able to move on to a simple test simulation of the metric involving diffusion in the ∇y-direction.

6.2 Simple Diffusion

In this short section we simulate the behaviour of simple diffusion parrallel to the magnetic field in the case of a rational q, and in the case of an irrational q.

The diffusion equation evaluated is simply

$$\partial_t N = D_{\parallel} \nabla_{\parallel}^2 N \tag{6.1}$$

where N is a particle density, and $D_{\parallel}$ is a constant.

Due to the shift in the z-coordinate being by $2\pi q\theta$ as seen in eq. (4.58) and the pseudo-periodicity expressed by eq. (4.60) we should see that for a rational q a magnetic field line will eventually close in on itself, where for an irrational q, the magnetic field line will never close in on itself, resulting in a magnetic field line covering a whole surface. This means that looking at two field lines for a choice of rational q with a different density on each field line, there should be no diffusion between the two field lines, where the opposite should be the case for an irrational choice of q.

Figure 6.4 shows diffusion at three different times with a diffusion constant of $D_{\parallel} = 1000$ and with a rational choice of q. The density is distributed, such that each field line has a constant density different from the other field line. As seen from the plots there is no diffusion from one field line to the other, just as expected.

Figure 6.5 shows diffusion at three different times with a diffusion constant of $D_{\parallel} = 1000$ and with an irrational choice of q and a distribution of density, such that each field line has a constant density different from the other field line. As expected the density evens out among the two field lines.

6.2.1 Cross-section and Interpolation

When investigating data it is often convenient to look at 2-dimensional cross sections with one coordinate held fixed. Imagine we want to look at a cross section of the data in toroidal coordinates at $\phi = 0$. If the simulation was done in a toroidal coordinate system with an equidistant grid, this would be straightforward, however, our simulations were done in a non-toroidal system, and the gridpoints are thus not necessarily uniformly distributed along a constant ϕ-plane. However there are various ways to interpolate data down to the poloidal plane in a toroidal geometry, and we simply use pythons built-in interpolator when processing the data[2].

In order to get results in a more visualizable coordinate system we map the data back to toroidal coordinates. We have a one-to-one map of the three field-aligned coordinates to toroidal coordinates, such that $(x_{fa}, y_{fa}, z_{fa}) \rightarrow (r, \eta, \phi)$, using the values for the toroidal coordinates in terms of the field-aligned coordinates we are able to map back to toroidal coordinates. This has been utilised in a simulation run using a 32x64x36 grid, with an initial distribution in the z-direction given by the function $N_0 = 1 + \sin(\frac{z}{2})$ in the range $]-\pi, \pi[$ for z, with diffusion in the y-direction, an irrational q and $D_\| = 1000$. Figure 6.6 shows the simulations for a cross section at $\phi = 0$ and $\phi = \pi$, where ϕ is the toroidal angle, at times 10 s, 4000 s and 20000 s. The figure shows that with time the density is evenly distributed as expected.

These simple diffusion tests have shown that the metric inputs behave as expected and that the results given in the field-aligned coordinates can be mapped back to a toroidal system, which validates our metric and numerical implementation.

[2]While the simulations where done using C++ and the BOUT++ [14] platform, the post processing was done in Python

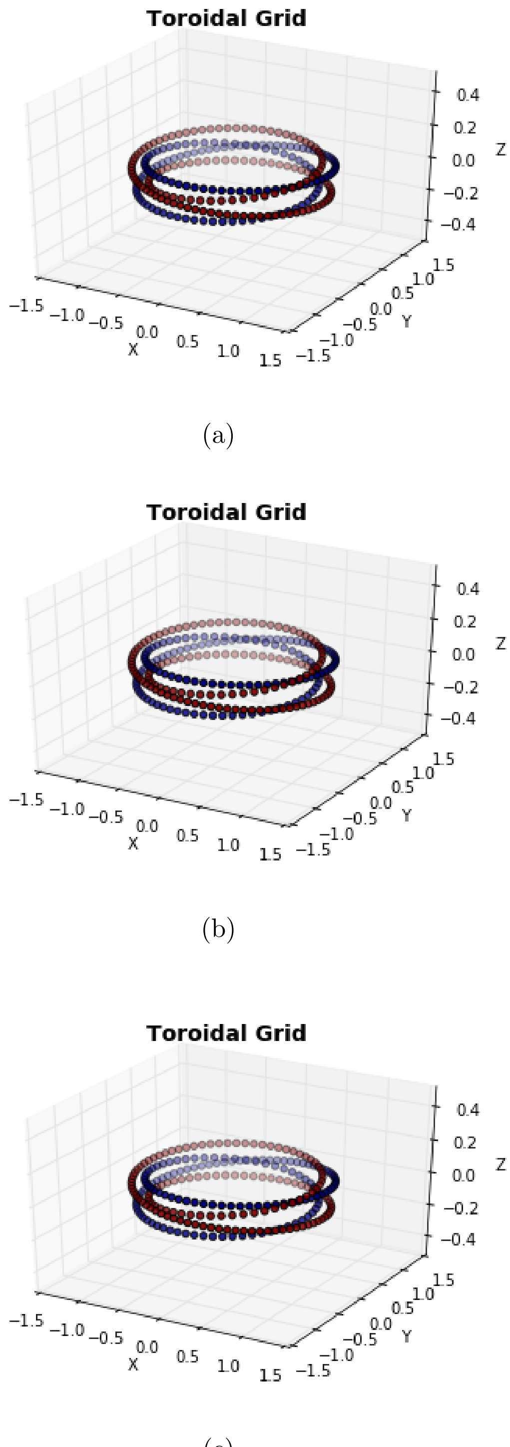

Figure 6.4: X, Y and Z in metres. At times $t = 20$ s, $t = 800$ s and $t = 4000$ s with $q = 2$

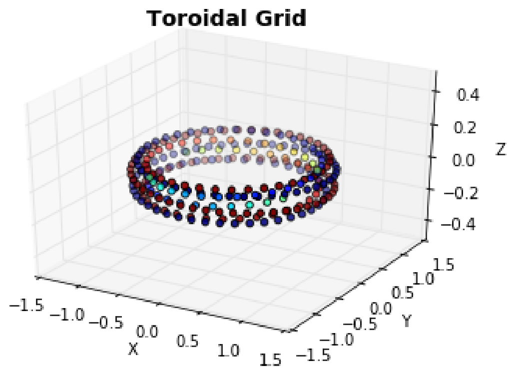

(a)

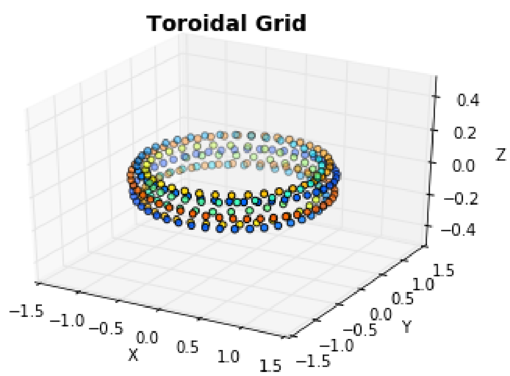

(b)

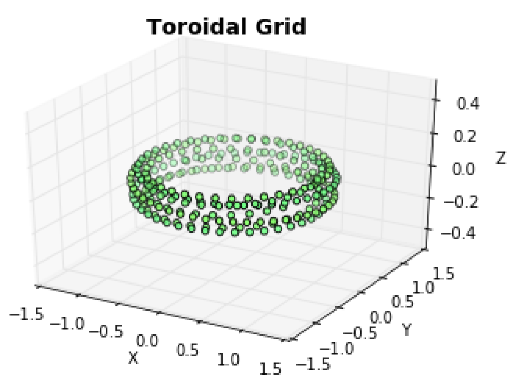

(c)

Figure 6.5: X, Y and Z in metres. At times $t = 20$ s, $t = 800$ s and $t = 4000$ s with $q = \pi$

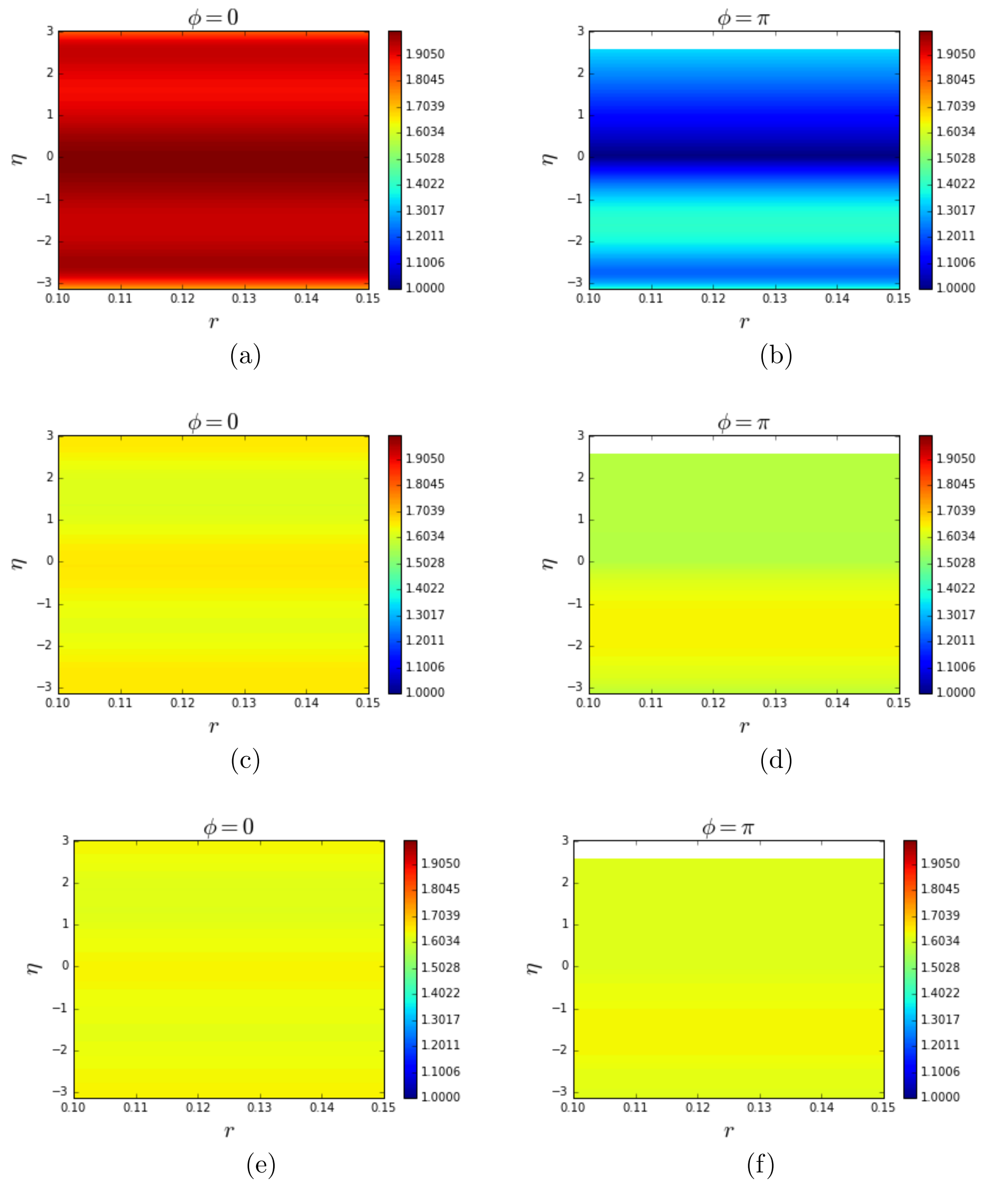

Figure 6.6: Diffusion along field lines at two different ϕ cross sections. At times $t = 10$ s, $t = 4000$ s, $t = 20000$ s from top to bottom and $q = \pi$

6.3 The Dispersion Relation and Unstable Modes

In order to investigate the growth rate of unstable modes it is convenient to look at the linearized limit of the Hasegawa-Wakatani equations. Doing this in a slab geometry is straightforward and gives a dispersion relation, however it is not straightforward in the field-aligned geometry used for the simulations performed in this chapter. Due to the complexity of the curvilinear coordinates we restrict our investigation to a slab geometry. This will give an indication of the growth-rates of the different modes in curvilinear geometry[3]. Slab geometry is defined as a cartesian coordinate system with y as the magnetic field axis[4].

When we assume that the geometry is a slab, the term $\mathbf{u}_E \cdot \nabla n_0$ can be rewritten to [16]

$$\mathbf{u}_E \cdot \nabla n_0 = \frac{1}{L_n B_0} \frac{\partial}{\partial z} \phi \tag{6.2}$$

The linearized Hasegawa-Wakatani equations are then [18]

$$\partial_t n + \partial_z \phi = -\mathcal{C} \partial_y^2 (\phi - n) + \mu \nabla_\perp^2 n \tag{6.3}$$
$$\partial_t \nabla_\perp^2 \phi = -\mathcal{C} \partial_y^2 (\phi - n) + \mu \nabla_\perp^4 \phi \tag{6.4}$$

where $\mathcal{C}$ is given by

$$\mathcal{C} = \frac{T_e L_n}{\eta e^2 n_0 \omega_{ci} \rho_s^3} \tag{6.5}$$

where the perpendicular length scales are normalized with ρ_s and the parallel length scales are normalized with L_n. The reason for this normalization is the different typical length scales perpendicular to the magnetic field and along the magnetic field.

Assuming plane wave solutions to eqns (6.3)-(6.4) and ignoring electron viscosity gives the dispersion relation [18]

[3]Things like magnetic shear, etc. are not included
[4]usually z, but BOUT++ uses y

$$\omega^2 + i\omega\left(\mathcal{C}k_y^2\left(1+\frac{1}{k_\perp^2}\right)+\mu k_\perp^2\right) - \mathcal{C}k_y^2\left(i\frac{k_z}{k_\perp^2}+\mu k_\perp^2\right) = 0 \tag{6.6}$$

In the limit where $\mathcal{C} \to \infty$ we get

$$\omega = \frac{k_z}{1+k_\perp^2} - i\frac{\mu k_\perp^4}{1+k_\perp^2} \tag{6.7}$$

The limit where $\mathcal{C} \to 0$ gives

$$\omega = -i\mu k_\perp^2, 0 \tag{6.8}$$

We see that both limits have a net negative of the imaginary parts, which results in a damping of the unstable modes [18]. This means that we have a stable solution in both limits, and furthermore that the limit where $\mathcal{C} \to \infty$ simply gives the standard result for drift waves in the z-direction [18].

The solution to the total dispersion relation is found to be

$$\omega = \frac{-i(\mathcal{C}k_y^2 k_\perp + \mu k_\perp^3 + \mathcal{C}k_y^2)}{2k_\perp} \pm \frac{\sqrt{-k_y^4(k_\perp+1)^2\mathcal{C}^2 + 2k_y^2\mathcal{C}(k_\perp^4\mu - k_\perp^3\mu) - \mu^2 k_\perp^6 + 4k_y^2\mathcal{C}i\omega^*}}{2k_\perp} \tag{6.9}$$

As seen the solution includes two branches, however the branch with $\Im(\omega) < 0$ is damped out by the negative imaginary part while the other branch is unstable, and drives the instabilities [18]. With $\mathcal{C} = 1$, $\mu = 0$ and $k_x = 0$, we plot the dispersion relation for the unstable branch ($\Im(\omega) > 0$) , which is illustrated in figure 6.7.

To better illustrate the growth-rate dependencies on k, we have plotted the cross sections of the imaginary frequency illustrated in figure 6.7 and in figure 6.8. As seen in the figure, the imaginary part (blue line) has a peak at a lower wave number for higher $\mathcal{C}$, and a faster decay after the peak. However for low $\mathcal{C}$ the peak of the imaginary part is at a lower frequency. This means that the peaks of both the real and imaginary parts go to zero for $\mathcal{C} \to 0$, and

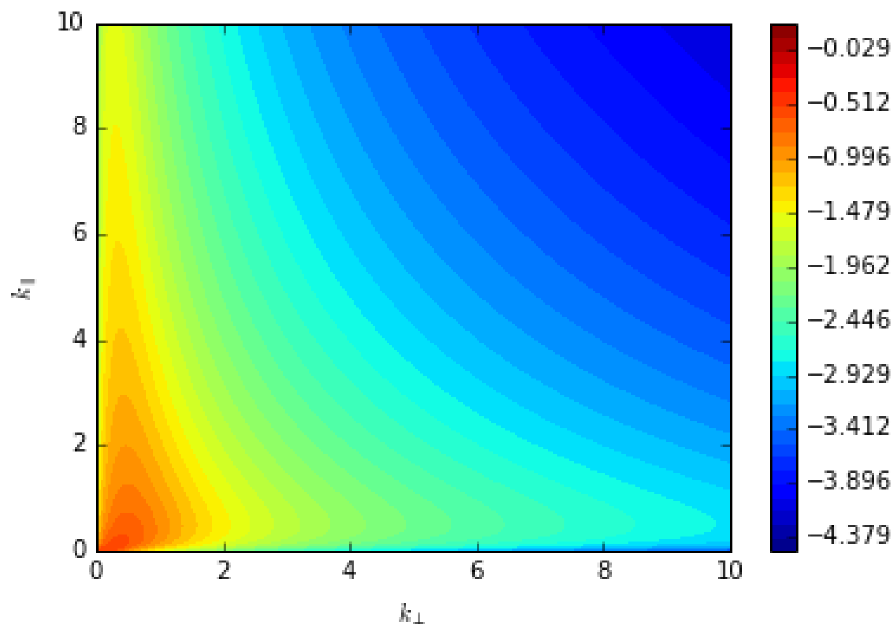

Figure 6.7: A contourplot of the imaginary part of the dispersion relation at $\mathcal{C} = 1$ and $\mu = 0$, with a logarithmic scale

the peak of the imaginary part goes to zero as $\mathcal{C} \to \infty$. The growth rate for the unstable modes is seen to have the maximum peak value around $\mathcal{C} = 1$.

Figure 6.9 shows the maximum frequency of the imaginary part of the perpendicular wave number, $k_\perp$, decaying fast for higher values of $\mathcal{C}$. For $\mathcal{C} \to 0$ the peak of both the real and the imaginary part goes to zero resulting in a stable solution.

Whilst this mainly tells us something about the Hasegawa-Wakatani model in a slab geometry, the results for a curvilinear geometry should be similar, with the drift wave instabilities peaking at a finite $\mathcal{C}$.

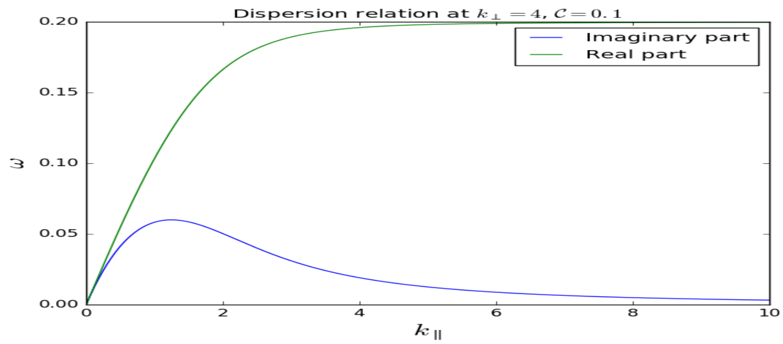

(a)

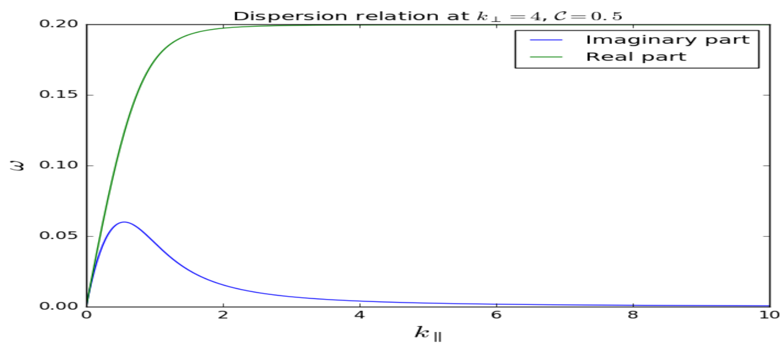

(b)

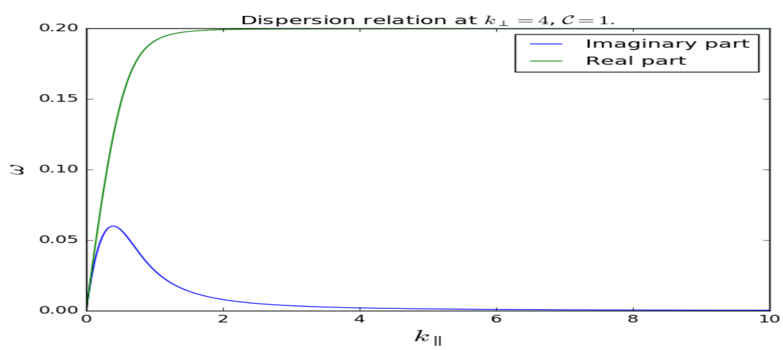

(c)

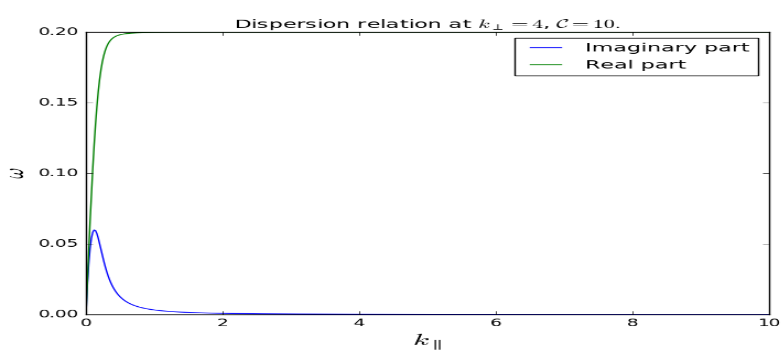

(d)

Figure 6.8: The dispersion relation at $k_\perp = 4$ for (a) $C = 0.1$, (b) $C = 0.5$, (c) $C = 1$ and (d) $C = 10$

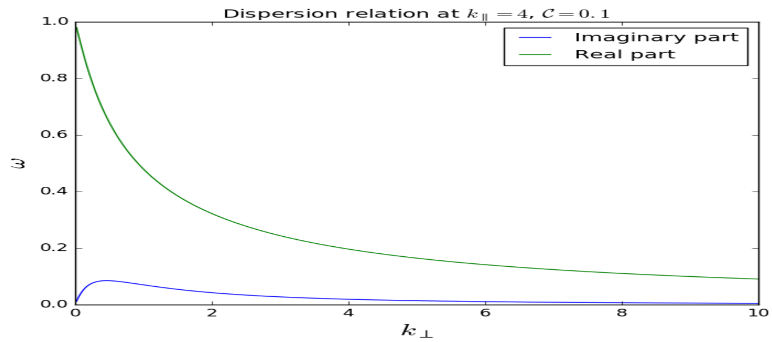

(a)

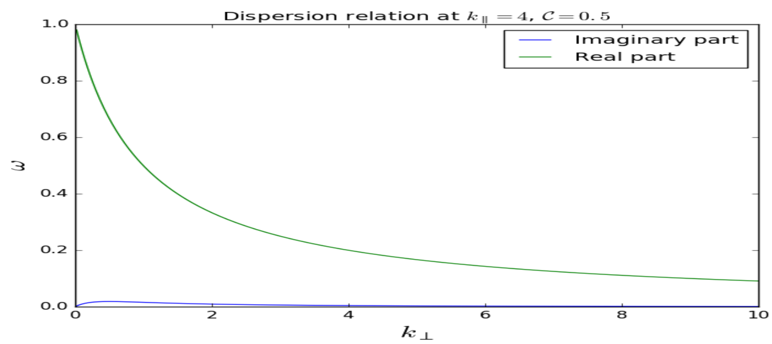

(b)

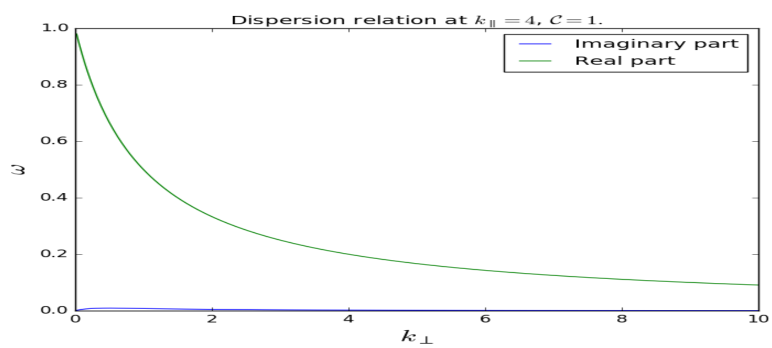

(c)

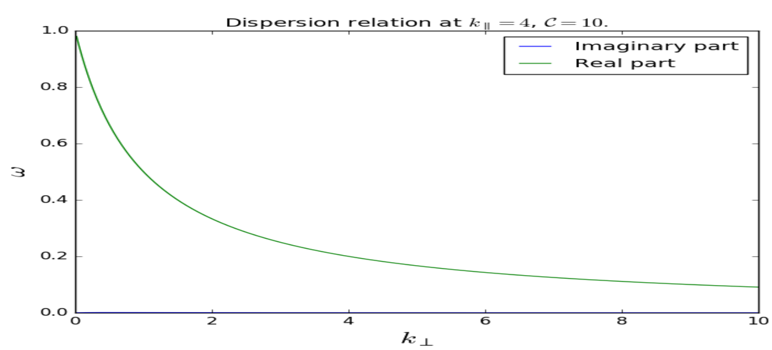

(d)

Figure 6.9: The dispersion relation at $k_{\parallel} = 4$ for (a) $C = 0.1$, (b) $C = 0.5$, (c) $C = 1$ and (d) $C = 10$

6.4 Numerical Simulations of The Hasegawa-Wakatani Model

With a theoretical idea of the stability of the Hasegawa-Wakatani equations, we now move on to analyze the results of simulations performed using the Hasegawa-Wakatani model in field-aligned coordinates. The simulations are investigated using three different values of magnetic shear (magnetic shear is defined as $s = \frac{r}{q}\frac{\partial q}{\partial r}$). We expect to see a dampening effect of the unstable modes in the system for high values of magnetic shear [20], which should also result in a net dampening of the total kinetic energy.

We define the total kinetic energy of the system [16]

$$\mathcal{E} = \mathcal{E}_{kin} = \frac{1}{2}\int\int\int((\nabla\phi)^2)dxdydz \tag{6.10}$$

where we use the numerical approximation

$$\int\int\int(f)dxdydz \approx \frac{1}{N_x N_y N_z}\sum_{x,y,z} f \tag{6.11}$$

where N_i denotes the number of grid points in the i-direction. It can be shown that the background density gradient $(\mathbf{u}_E \cdot \nabla \ln(n_0))$ acts as a source term for the energy of the system [16].

6.4.1 Numerical Simulations With Magnetic Shear

The value of $\mathcal{C}$ can be calculated for specific values of electron temperature, ω_{ci}, n_0 and η. The given values can be seen on table 6.2

Recalling that

$$\mathcal{C} = \frac{T_e}{\eta e^2 n_0 \omega_{ci} \rho_s^2}$$

we get a value of $\mathcal{C} = 356000$.

For our initial value at $t = 0$ we use an initial spread in vorticity given by the function $0.0001(mixmode(y) \cdot mixmode(z) \cdot mixmode(2\pi x))$, where the mixmode function is a mixture of fourier modes on the form [12]

Table 6.2: Values used for the simulation

	symbol	value
Particle background number density	n_0	10^{19}
Electron temperature	T_e	100 eV
The ion cyclotron frequency	ω_{ci}	47904191 s^{-1}
The plasma resisitivity	η	$1.7 \cdot 10^{-6}$
The ion larmor radiues at electron temperature T_e	ρ_s	0.0014 m
The electron charge	e	$1.6 \cdot 10^{-19}$ C
The background magnetic field	B_0	1 T

$$mixmode(x) = \sum_{i=1}^{14} \frac{1}{(1 + |i - 4|)^2} \cos[ix + \phi], \tag{6.12}$$

where ϕ is a random phase between -π and π. The boundaries in the y- and z-directions are periodic and on the x-coordinates boundaries we impose dirichlet boundaries[5] [19] of values 0. The same boundaries are applied to the normalized density n. The grid used is an equidistant $66 \times 16 \times 512$ grid using the field-aligned coordinates derived in chapter 4, with input parameters for the metric and coordinates given in table 6.1. The timestep used was $\tilde{t} = 100$ corresponding to $t = \frac{100}{\omega_{ci}}$. The background density gradient was set to be $\nabla(\log(n_0)) = \nabla(-1 \cdot x)$.

Figure 6.10 shows the total normalised kinetic energy in the system as a function of time with and without kinetic energy in the parallel direction. As seen from the plot the kinetic energy in the parallel direction contributes with almost nothing, which means the drift waves and turbulence mainly results in motion perpendicular to the magnetic field.

At approximately $\tilde{t} = 800$ the kinetic energy of the system starts growing exponentially up untill approximately $\tilde{t} = 8700$. In this region the kinetic energy is concentrated in the stable wave numbers, with a resulting drift in the z-direction. A snapshot during this time period at a cross section of $y = 0.25\pi$ can be seen in figure 6.11.

[5]For the finite difference methods used in BOUT++ see [19] and [12]

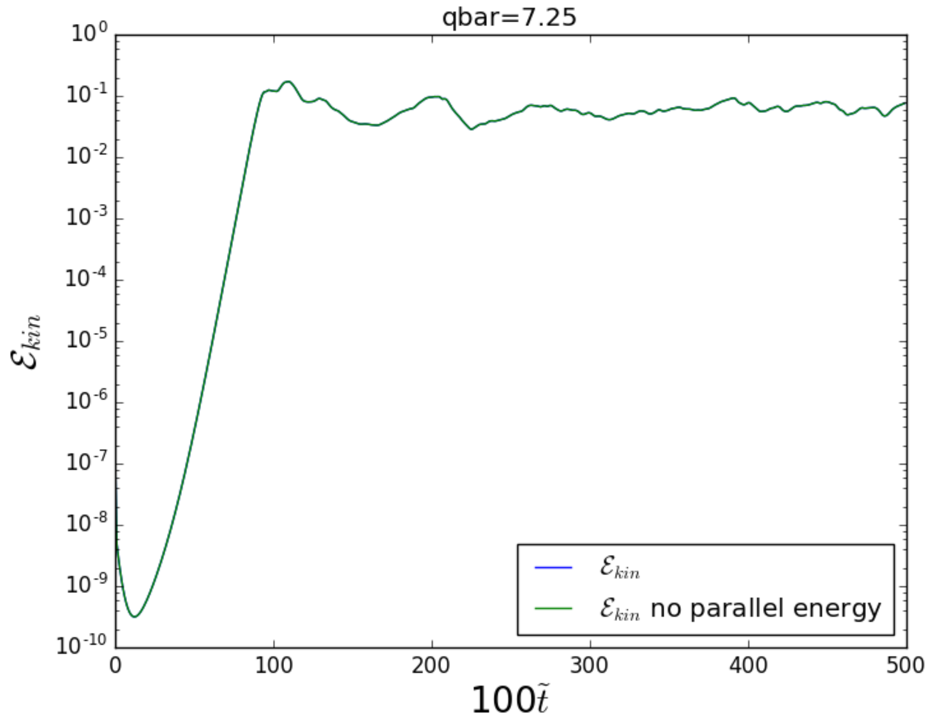

Figure 6.10: The kinetic energy as a function of time.

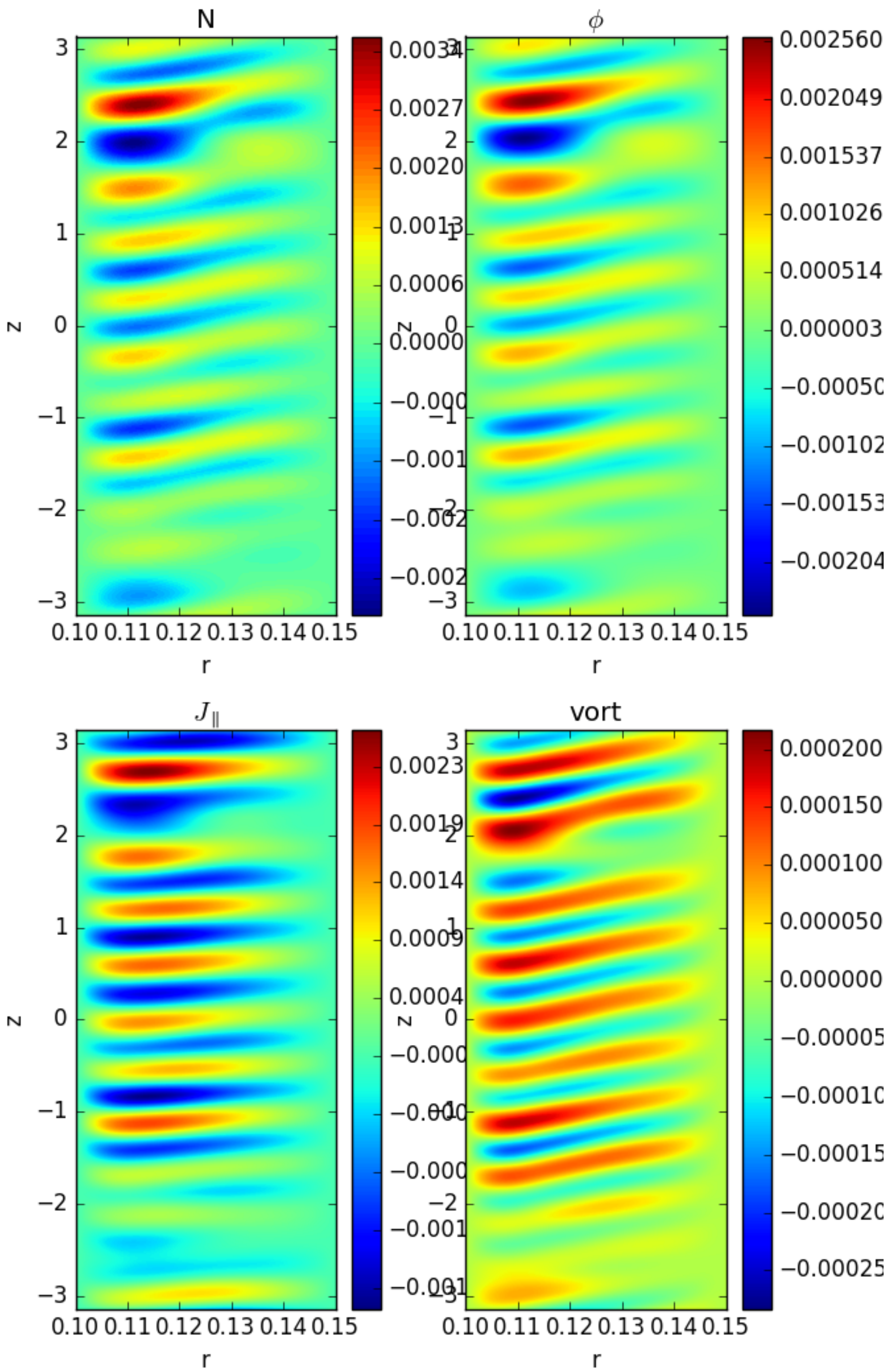

Figure 6.11: The normalized values for n, ϕ ,$\nabla^2\phi$ and $J_{\|}$ at time $\tilde{t} = 6000$ with $\frac{\partial q}{\partial r} = 7.25$

The period from time $\tilde{t} = 8700$ and onward denotes the state of the system where the total kinetic energy of the system is saturated. In the saturated state the system becomes turbulent and random oscillations in the total kinetic energy are observed. Figure 6.12 shows a snapshot during the start of the turbulent time period at a cross section of $y = 0.25\pi$. Figure 6.13 shows a snapshot well into the turbulent time period at a cross section of $y = 0.25\pi$. As seen in figure 6.13 it seems that ϕ goes in to a state with elongated modes late in the turbulent time period.

As mentioned earlier the magnetic shear is expected to have a positive influence on the stability of the system. In order to investigate this influence, we compare these results to a system with no magnetic shear and a system with stronger magnetic shear.

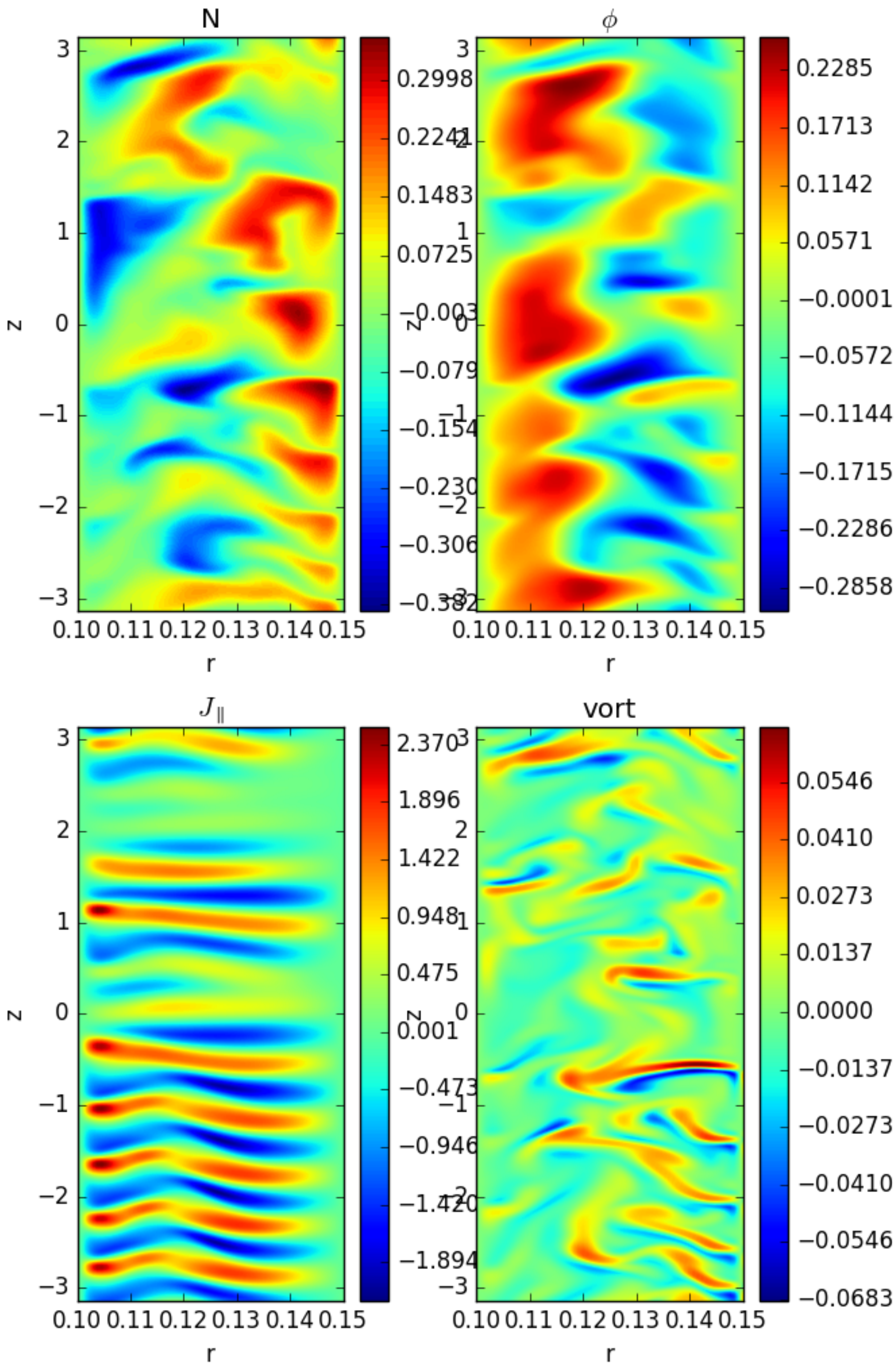

Figure 6.12: The normalized values for n, ϕ ,$\nabla^2\phi$ and $J_\parallel$ at time $\tilde{t} = 10600$ with $\frac{\partial q}{\partial r} = 7.25$

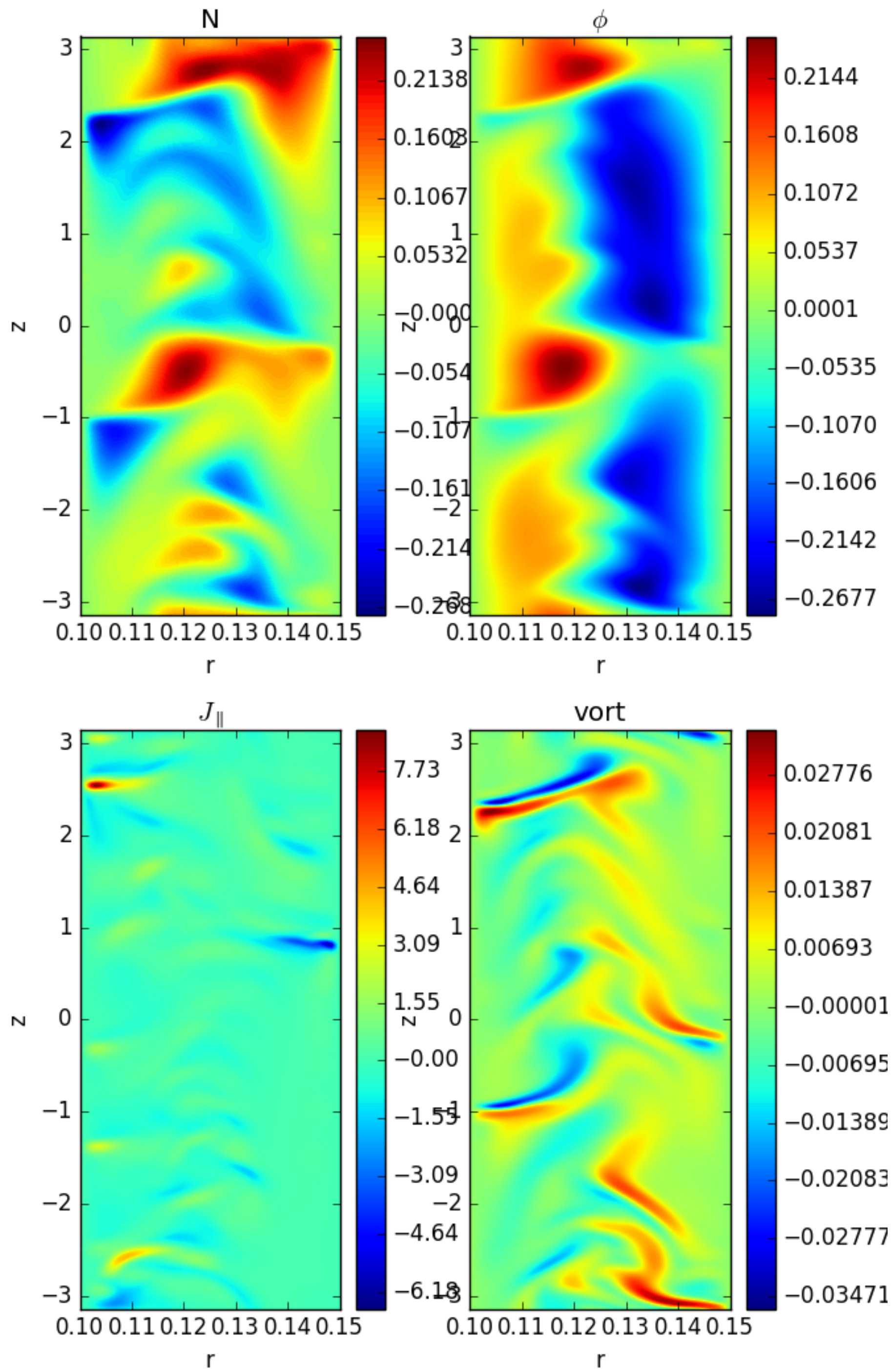

Figure 6.13: The normalized values for n, ϕ ,$\nabla^2\phi$ and $J_\parallel$ at time $\tilde{t} = 35000$ with $\frac{\partial q}{\partial r} = 7.25$

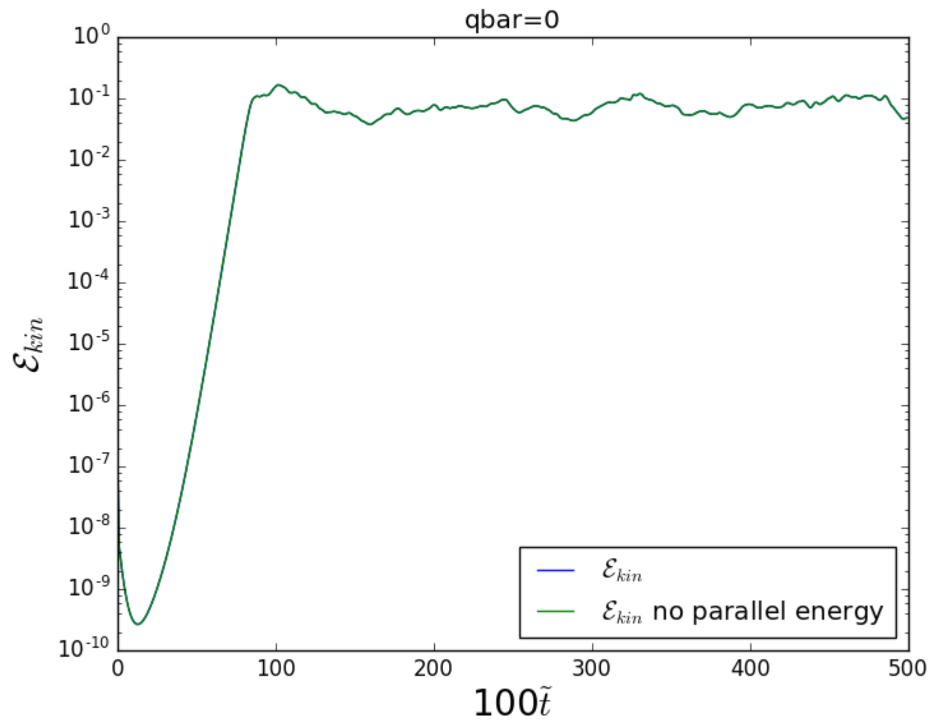

Figure 6.14: The kinetic energy as a function of time.

Comparisons with no magnetic shear

In this subsection we investigate the case where no magnetic shear is present, that is we set $\frac{\partial q}{\partial r} = 0$, whilst not changing any other parameters. What we expect is a less stable Hasegawa-Wakatani system, that reaches a saturated state faster than a Hasegawa-Wakatani system with shear. We also expect higher total kinetic energy in the saturated state due to more unstable motion.

Figure 6.14 shows the total normalized kinetic energy of the system with no shear. At approximately $\tilde{t} = 800$ the kinetic energy of the system starts growing exponentially up untill approximately $\tilde{t} = 8000$. Compared to the previous simulation it reaches the saturated state a bit faster. By zooming in at time $\tilde{t} = (30000 - 45000)$ for the total kinetic energy with and without magnetic shear we get figures 6.15 for no magnetic shear, and figure 6.16 for the case with magnetic shear. It is quite clear that the total kinetic energy

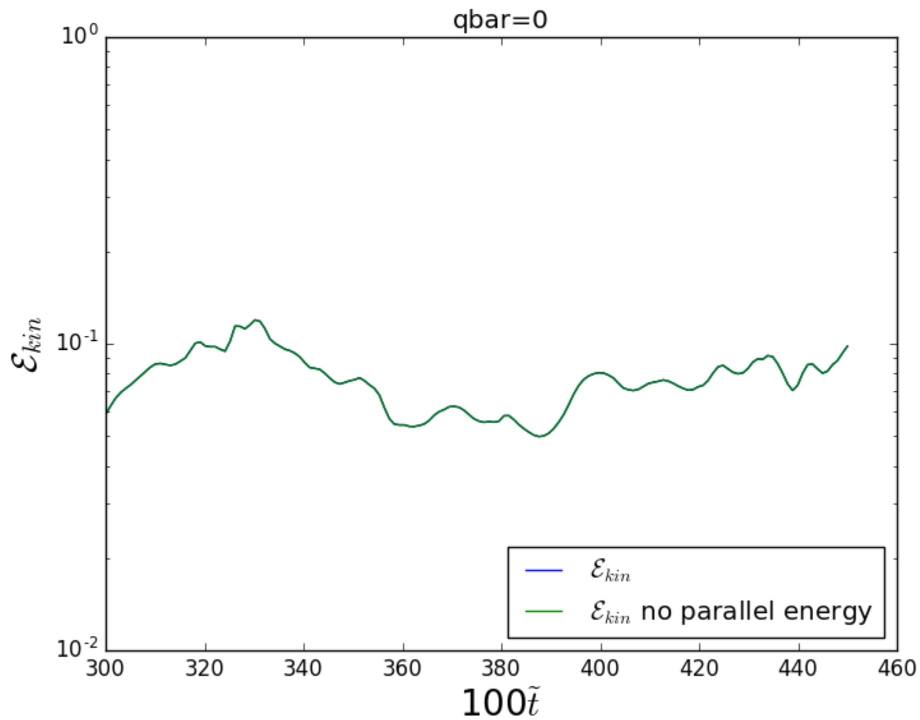

Figure 6.15: The kinetic energy as a function of time.

in the saturated state in the case with no magnetic shear is larger.

Figure 6.17 shows the system with no shear at time $\tilde{t} = 6000$ and $y = 0.25\pi$. Comparing figure 6.17 with figure 6.11 it is seen that the density profile, the electric potential and the vorticity is shifted in the z-direction for higher r when magnetic shear is present, whereas it is not shifted in the case without magnetic shear.

Figure 6.18 shows the system with no magnetic shear at the initial state of the turbulent time period and figure 6.19 shows the same system well into the turbulent time period, both at $y = 0.25\pi$. Compared to the system with shear, ϕ does not seem to form the same elongated modes.

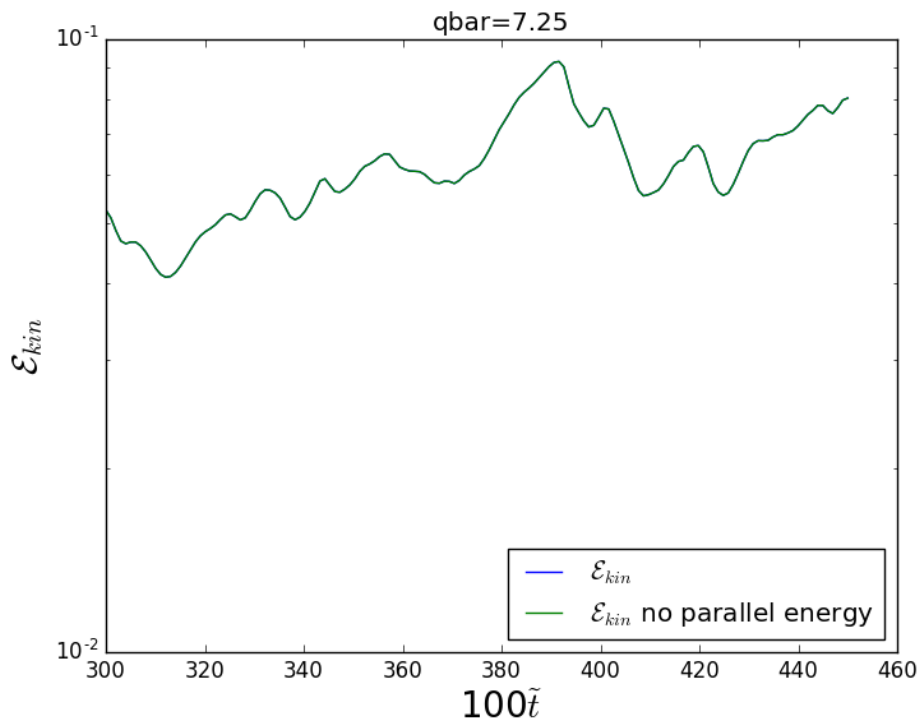

Figure 6.16: The kinetic energy as a function of time.

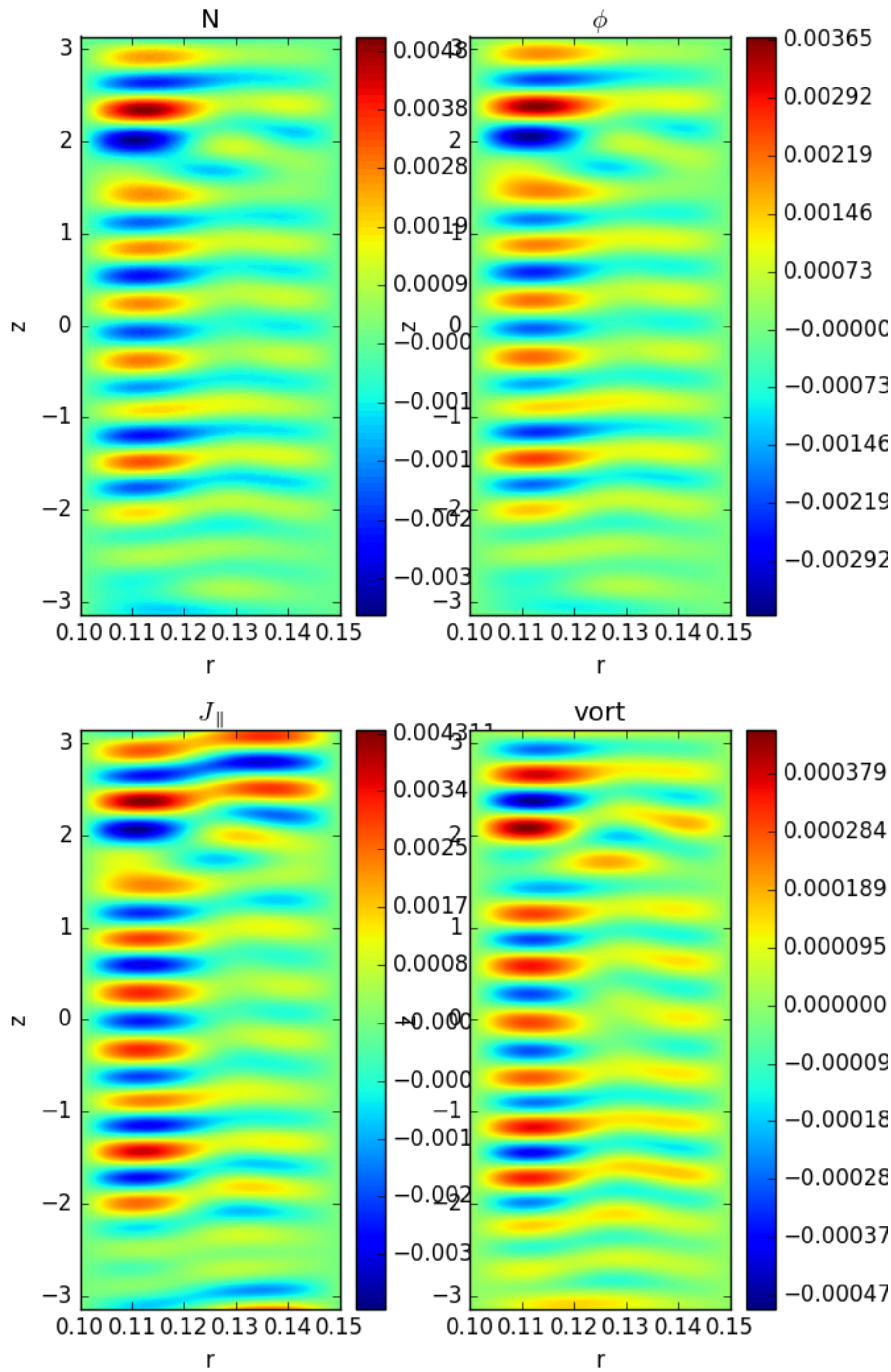

Figure 6.17: The normalized values for n, ϕ ,$\nabla^2\phi$ and $J_\parallel$ at time $\tilde{t} = 6000$ with $\frac{\partial q}{\partial r} = 0$

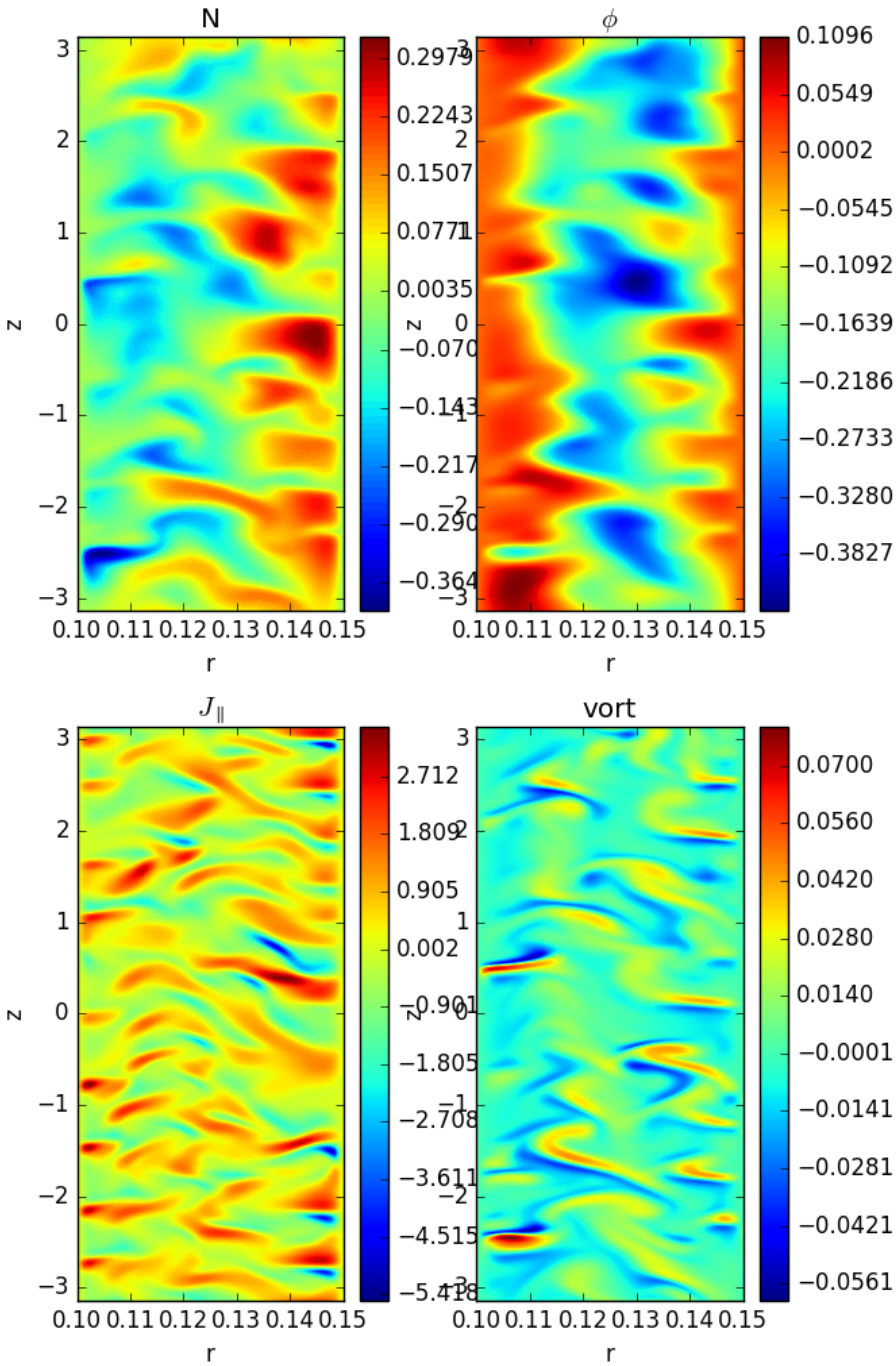

Figure 6.18: The normalized values for n, ϕ ,$\nabla^2\phi$ and $J_\parallel$ at time $\tilde{t} = 10600$ with $\frac{\partial q}{\partial r} = 0$

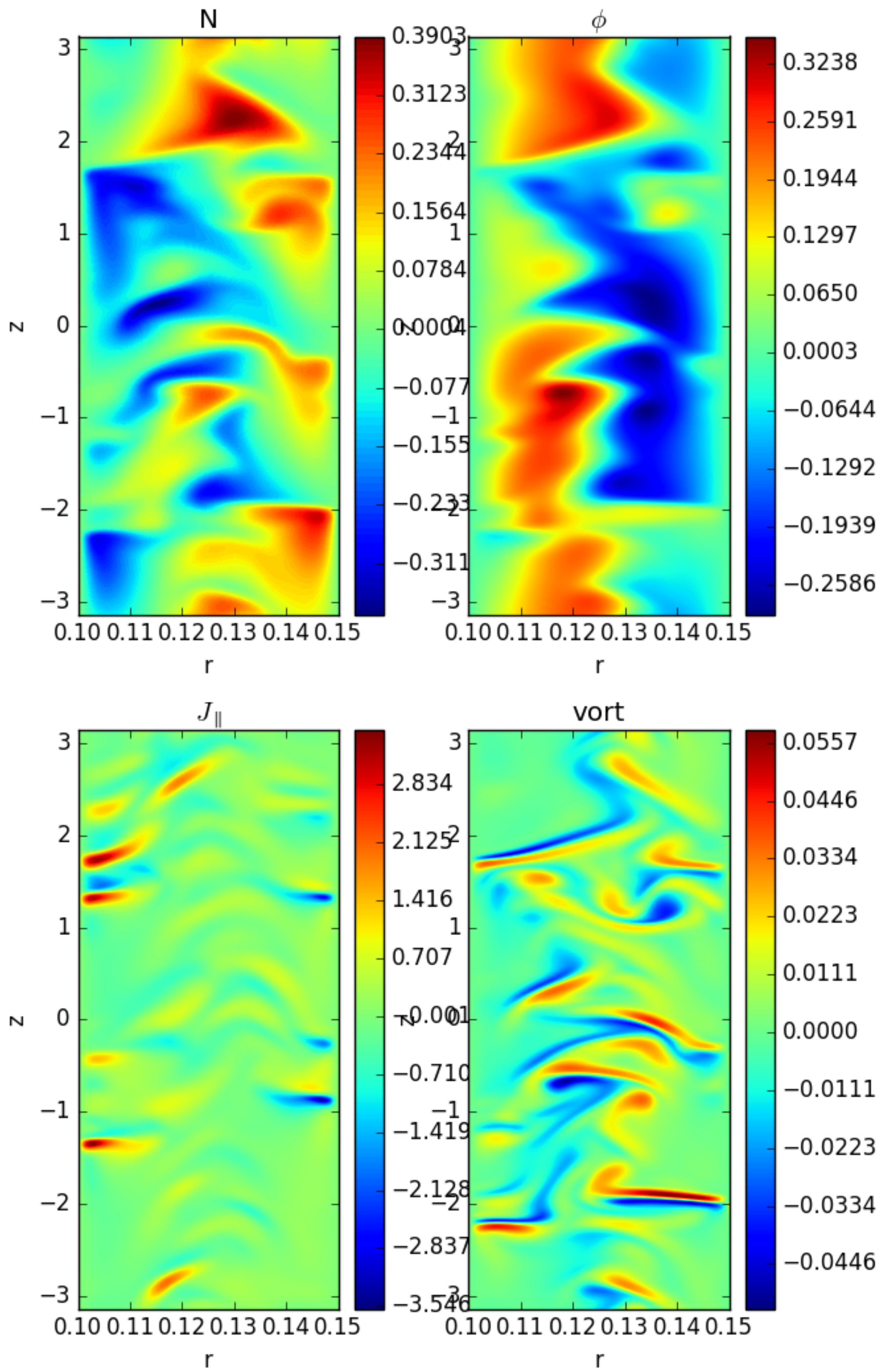

Figure 6.19: The normalized values for n, ϕ ,$\nabla^2\phi$ and $J_\parallel$ at time $\tilde{t} = 35000$ with $\frac{\partial q}{\partial r} = 0$

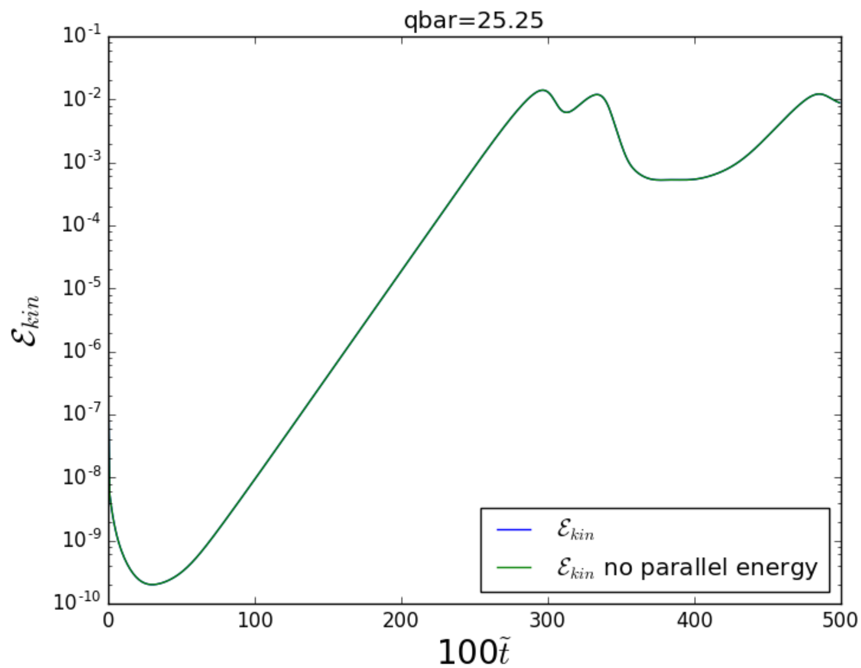

Figure 6.20: The kinetic energy as a function of time.

Comparison with strong magnetic shear

We now move on to investigate the case with strong magnetic shear where $\frac{\partial q}{\partial r} = 25.25$. The other values used for the simulation are the same as for the case with no magnetic shear, and the case with weaker magnetic shear.

Figure 6.20 shows the total normalized kinetic energy of the system with strong magnetic shear. At approximately $\tilde{t} = 800$ the kinetic energy of the system starts growing up untill approximately $\tilde{t} = 27000$. This is a significant difference from the case with no magnetic shear and the case with weaker magnetic shear. Furthermore the saturation level of the total normalized kinetic energy is a factor 10 lower than in the previous cases examined. The fluctuations in the kinetic energy in the saturated state are much less frequent than in the case with no magnetic shear and the case with weaker magnetic shear.

Figure 6.21 shows the system in the drift wave time period at $y = 0.25\pi$. The shear is clearly seen in the density profile, the vorticity and the electric potential.

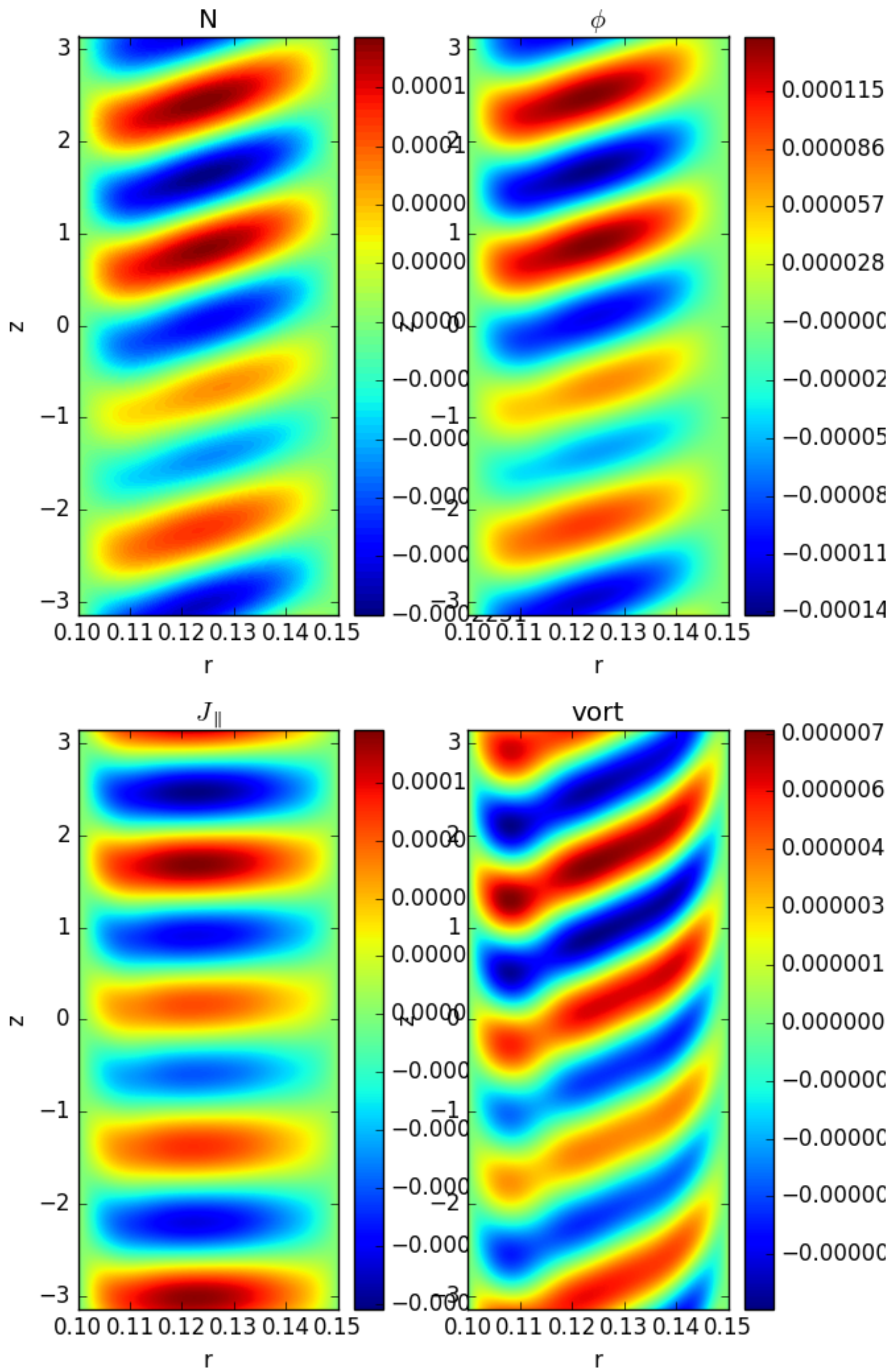

Figure 6.21: The normalized values for n, ϕ ,$\nabla^2\phi$ and $J_\parallel$ at time $\tilde{t} = 10600$ with $\frac{\partial q}{\partial r} = 25.25$

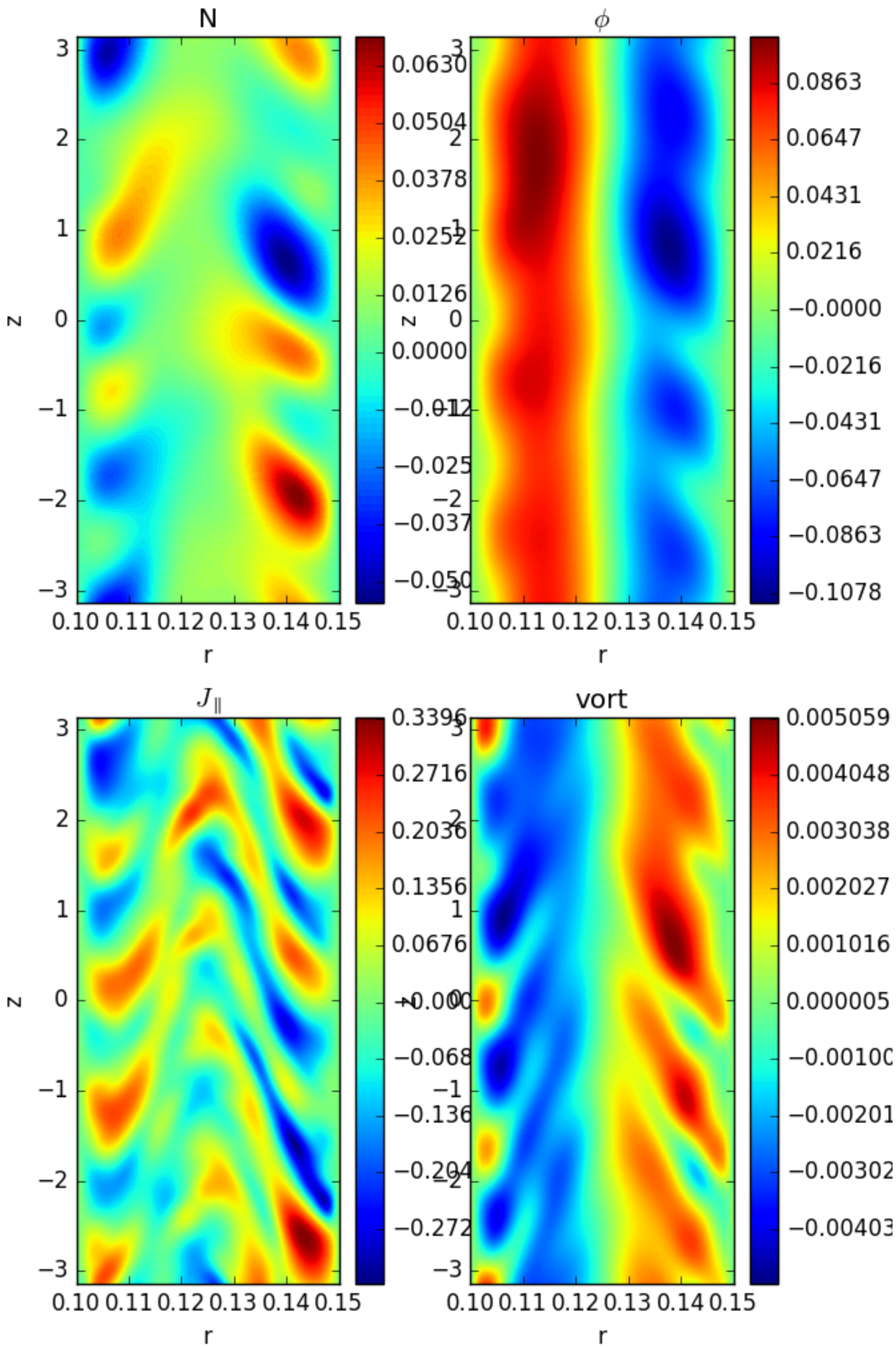

Figure 6.22: The normalized values for n, ϕ ,$\nabla^2\phi$ and $J_{\|}$ at time $\tilde{t} = 35000$ with $\frac{\partial q}{\partial r} = 25.25$

Figure 6.22 shows the system in the turbulent time period at $y = 0.25\pi$ the elongated modes in the electric potential are even more visible now.

It is clear that the magnetic shear has a stabilizing effect on the system and this can be utilized when building a fusion plasma device.

Chapter 7

Conclusion

In order to accurately describe a fusion plasma 3D effects of the magnetic field must be taken in to account. A 3D model using a coordinate system aligned with the magnetic field takes these effects in to account and leads to high resolution of the effects with a coarse grid in the magnetic field line direction.

To create a 3D model of a fusion plasma the shape of the magnetic field was described in detail, from which a coordinate system aligned with the magnetic field was derived. A metric, involving all necesarry information about the magnetic field structure, was created from the field-aligned coordinates. The Hasegawa-Wakatani model was then investigated using the field-aligned coordinate system.

A simple diffusion test was carried out in order to validate the model and prove the ability of mapping the results in field-aligned coordinates back to a toroidal coordinate system.

Simulations involving three different cases of the derived equations were investigated using the BOUT++ [14] platform for writing the code, one with a magnetic shear of $\frac{\partial q}{\partial r} = 7.25$, one with no shear and one with a shear of $\frac{\partial q}{\partial r} = 25.25$. Significant differences were seen, where the magnetic shear was shown to have a stabilizing effect on the system.

The 3D model showed promising results as a basis for future simulations in three dimensions.

7.1 Future Prospects

Creating a coordinate system aligned with the magnetic field is a complicated and tedious affair, however with this succesfully done, and immediate effects resulting from the properties of the magnetic field seen, the 3D model created in this thesis seems to be a great basis for future work using a field aligned system.

The model investigated in this thesis was the simplified Hasegawa-Wakatani model which includes assumptions such as zero ion temperature, which does not necesarrily hold in real fusion devices. Future works may be done using more complex systems involving finite ion temperature and other neglected effects, such as temperature gradients and parallel ion velocity.

During the simulations, the local approximation was used, which only holds for flat gradients or a very thin slab in the r-direction. Future works may want to include global effects of r and a first step could be to investigate the differences between a model using the local approximation and a global model.

The 3D model used for the simulations assumed a circle equilibrium solution to the Grad-Shafranov equation in order to have an analytical expression for the field-aligned metric. However this holds an inconsistency of $O(\epsilon)$ with $\epsilon = \frac{r}{R_0}$ and future works may set out to investigate more complex models with more realistic solutions to the Grad-Shafranov equation.

Appendix A

Toroidal Metric Coefficients

Using the Cartesian metric where

$$g^{xx} = 1 \tag{A.1}$$
$$g^{yy} = 1 \tag{A.2}$$
$$g^{zz} = 1 \tag{A.3}$$

and the off-diagonal terms are 0 it is pretty straightforward to determine the metric for a toroidal coordinate system. Defining the coordinates we have:

$$x = (R_0 + r\cos(\eta))\sin(\phi) \tag{A.4}$$
$$y = (R_0 + r\cos(\eta))\cos(\phi) \tag{A.5}$$
$$z = r\sin(\eta), \tag{A.6}$$

where x, y and z are the usual Cartesian coordinates, R_0 is the major radius, r is the minor radius, η is the poloidal angle and ϕ is the toroidal angle.

Writing the set of toroidal coordinates in terms of cartesian coordinates we solve the three equations with three unknowns.

$$\phi = \arcsin(\frac{x}{R_0 + r\cos(\eta)}) \tag{A.7}$$

so

$$y = (R_0 + r\cos(\eta))\cos(\arcsin(\frac{x}{R_0 + r\cos(\eta)})) \tag{A.8}$$

using

$$\cos(\arcsin(x)) = \sqrt{1 - x^2} \tag{A.9}$$

we have

$$y = (R_0 + r\cos(\eta))\sqrt{1 - \frac{x^2}{(R_0 + r\cos(\eta))^2}} \tag{A.10}$$

$$= \sqrt{(R_0 + r\cos(\eta))^2 - x^2} \Rightarrow \tag{A.11}$$

$$y^2 = (R_0 + r\cos(\eta))^2 - x^2 \Rightarrow \tag{A.12}$$

$$r\cos(\eta) = \sqrt{x^2 + y^2} - R_0 \Rightarrow \tag{A.13}$$

$$\eta = \arccos(\frac{\sqrt{x^2 + y^2} - R_0}{r}). \tag{A.14}$$

This allows us to find a solution for r using eq. (A.6) and the rule given in eq. (A.9):

$$r = \frac{z}{\sqrt{1 - (\frac{\sqrt{x^2+y^2} - R_0}{r})^2}} \Rightarrow \tag{A.15}$$

$$r^2 = z^2 + (\sqrt{x^2 + y^2} - R_0)^2 \tag{A.16}$$

we then plug in to the equation for η and have

$$\eta = \arccos(\frac{\sqrt{x^2 + y^2} - R_0}{\sqrt{z^2 + (\sqrt{y^2 + x^2} - R_0)^2}}) \tag{A.17}$$

which then gives for ϕ

$$\sin(\phi) = \frac{x}{\sqrt{x^2 + y^2}}. \tag{A.18}$$

We now find the gradient of the resulting expressions. Taking the gradient on both sides of r^2 we have

$$2r\nabla r = 2z\hat{z} + \frac{2(\sqrt{x^2+y^2} - R_0)y}{\sqrt{x^2+y^2}}\hat{y} + \frac{2(\sqrt{x^2+y^2} - R_0)x}{\sqrt{x^2+y^2}}\hat{x} \tag{A.19}$$

Taking the gradient on both sides for $\cos(\eta)$ we have

$$-\sin(\eta)\nabla\eta = \frac{xz^2\hat{x} + yz^2\hat{y} + (\sqrt{x^2+y^2} - R_0)z\sqrt{x^2+y^2}\,\hat{z}}{(z^2 + (\sqrt{y^2+x^2} - R_0)^2)^{\frac{3}{2}}\sqrt{x^2+y^2}} \tag{A.20}$$

Finally taking the gradient on both sides of $\sin(\phi)$ gives

$$\cos(\phi)\nabla\phi = \frac{y^2\hat{x} + xy\hat{y}}{(x^2+y^2)^{\frac{3}{2}}} \tag{A.21}$$

The derived expressions allows us to derive the metric of the torusoidal geometry. Using

$$g^{ij} = \nabla\mathbf{u}^i \cdot \nabla\mathbf{u}^j \tag{A.22}$$

we have

$$\begin{aligned} g^{rr} = \nabla r \cdot \nabla r &= \frac{z^2}{r^2} + \frac{(y^2+x^2)}{r^2}\left(\frac{(\sqrt{x^2+y^2} - R_0)^2}{x^2+y^2}\right) \\ &= \sin^2(\eta) + \frac{(R_0 + r\cos(\eta))^2}{r^2}\left(\frac{(r\cos(\eta))^2}{(R_0 + r\cos(\eta))^2}\right) = 1 \end{aligned} \tag{A.23}$$

and

$$\begin{aligned} g^{\eta\eta} &= \frac{1}{\sin^2(\eta)}\left(\frac{(x^2+y^2)(z^4 + (\sqrt{x^2+y^2} - R_0)^2 z^2)}{(x^2+y^2)(z^2 + (\sqrt{x^2+y^2} - R_0)^2)^3}\right) \\ &= r^2\left(\frac{1}{(r^2\sin^2(\eta) + r^2\cos^2(\eta))^2}\right) = \frac{1}{r^2} \end{aligned} \tag{A.24}$$

and for the last non-zero metric element we have

$$
\begin{aligned}
g^{\phi\phi} &= \frac{1}{\cos^2(\phi)}\left(\frac{y^2(x^2+y^2)}{(x^2+y^2)^3}\right) \\
&= \frac{1}{R^2},
\end{aligned}
\tag{A.25}
$$

where $R = R_0 + r\cos(\eta)$ and the Jacobian is $\frac{1}{rR}$.

Appendix B

Useful Vector Identities

In this section a list of useful vector identities is stated.

Vector dot product:

$$\nabla(\mathbf{A}\cdot\mathbf{B}) = (\mathbf{A}\cdot\nabla)\mathbf{B} + (\mathbf{B}\cdot\nabla)\mathbf{A} + \mathbf{A}\times(\nabla\times\mathbf{B}) + \mathbf{B}\times(\nabla\times\mathbf{A}) \tag{B.1}$$

Vector cross product

$$\nabla\cdot(\mathbf{A}\times\mathbf{B}) = (\nabla\times\mathbf{A})\cdot\mathbf{B} - \mathbf{A}\cdot(\nabla\times\mathbf{B}) \tag{B.2}$$

$$\nabla\times(\mathbf{A}\times\mathbf{B}) = \mathbf{A}(\nabla\cdot\mathbf{B}) - \mathbf{B}(\nabla\cdot\mathbf{A}) + (\mathbf{B}\cdot\nabla)\mathbf{A} - (\mathbf{A}\cdot\nabla)\mathbf{B} \tag{B.3}$$

The vector triple product

$$\mathbf{A}\times(\mathbf{B}\times\mathbf{C}) = (\mathbf{A}\cdot\mathbf{C})\,\mathbf{B} - (\mathbf{A}\cdot\mathbf{B})\,\mathbf{C} \tag{B.4}$$

$$(\mathbf{A}\times\mathbf{B})\times\mathbf{C} = (\mathbf{A}\cdot\mathbf{C})\,\mathbf{B} - (\mathbf{B}\cdot\mathbf{C})\,\mathbf{A} \tag{B.5}$$

The divergence of a scalar and a vector

$$\nabla\cdot(\psi\mathbf{A}) = \psi\nabla\cdot\mathbf{A} + \mathbf{A}\cdot\nabla\psi \tag{B.6}$$

The curl of a scalar and a vector

$$\nabla\times(\psi\mathbf{A}) = \psi\nabla\times\mathbf{A} + \nabla\psi\times\mathbf{A} \tag{B.7}$$

Bibliography

[1] J. Goldemberg, United Nations Development Programme, United Nations. Dept. of Economic, Social Affairs, and World Energy Council. *World energy assessment: energy and the challenge of sustainability*. United Nations Development Programme, 2000.

[2] K.S. Krane. *Introductory Nuclear Physics*. Wiley, 1987.

[3] M. P. Lucas, L. L. & Unterweger. Comprehensive review and critical evaluation of the half-life of tritium. *Journal of Research of the National Institute of Standards and Technology*, 105, 2000.

[4] J. Wesson and D.J. Campbell. *Tokamaks*. International Series of Monographs on Physics. OUP Oxford, 2011.

[5] George M. Hornberger. New manuscript guidelines for the reporting of stable hydrogen, carbon, and oxygen isotope ratio data. *Water Resources Research*, 31(12):2895–2895, 1995.

[6] R. Fitzpatrick. *Plasma Physics: An Introduction*. Taylor & Francis, 2014.

[7] Internal workings of a conventional tokamak with a central solenoid. credit: Max-planck institut fr plasmaphysik. `http://www.100milliondegrees.com/merging-compression/`. Accessed: 2016-11-25.

[8] M.S. Tillack, A.D. Turnbull, C.E. Kessel, N. Asakura, A.M. Garofalo, C. Holland, F. Koch, Ch. Linsmeier, S. Lisgo, R. Maingi, R. Majeski, J. Menard, F. Najmabadi, R. Nygren, T.D. Rognlien, D.D. Ryutov, R.D. Stambaugh, P.C. Stangeby, and D.P. Stotler. Summary of the aries town

meeting: edge plasma physics and plasma material interactions in the fusion power plant regime. *Nuclear Fusion*, 53(2):027003, 2013.

[9] P.M. Bellan. *Fundamentals of Plasma Physics*. Cambridge University Press, 2008.

[10] W.D. D'haeseleer. *Flux coordinates and magnetic field structure: a guide to a fundamental tool of plasma structure*. Springer series in computational physics. Springer-Verlag, 1991.

[11] P. Helander and D.J. Sigmar. *Collisional Transport in Magnetized Plasmas*. Cambridge Monographs on Plasma Physics. Cambridge University Press, 2005.

[12] B D Dudson, M V Umansky, X Q Xu, P B Snyder, and H R Wilson. User manual for BOUT++. *Computer Physics Communications*, 180:1467–1480, 2009.

[13] Tiago Ribeiro. *Low frequency turbulence in the scrape-off layer of tokamak plasmas*. PhD thesis, Max Planck Institute for Plasma Physics, 2006.

[14] B D Dudson, M V Umansky, X Q Xu, P B Snyder, and H R Wilson. BOUT++: A framework for parallel plasma fluid simulations. *Computer Physics Communications*, 180:1467–1480, 2009.

[15] Toroidal coordinates. `http://fusionwiki.ciemat.es/fusionwiki/images/1/10/Toroidal_coordinates.png`. Accessed: 2016-11-25.

[16] Sren B Korsholm. *Coherent structures and transport in drift wave plasma turbulence*. PhD thesis, Technical University of Denmark, 2006.

[17] Akira Hasegawa and Masahiro Wakatani. Plasma edge turbulence. *Phys. Rev. Lett.*, 50:682–686, Feb 1983.

[18] Hans L. Pecseli. *Waves and Oscillations in Plasmas*. Series in plasma physics. CRC Press, 2013.

[19] R.J. LeVeque. *Finite Difference Methods for Ordinary and Partial Differential Equations: Steady-State and Time-Dependent Problems*. SIAM e-books. Society for Industrial and Applied Mathematics (SIAM, 3600 Market Street, Floor 6, Philadelphia, PA 19104), 2007.

[20] Paul H. Rutherford and Edward A. Frieman. Stabilization of drift waves by shear. *Physics of Fluids*, 10(5):1007–1016, 1967.